8

Energy-Harvesting Systems

8.1 Introduction to Energy-Harvesting Systems

Research on energy-harvesting applications has gained importance in the last decade [1–10]. The most commonly discussed applications include wireless sensor nodes for healthcare, embedded or implanted sensor nodes for medical applications, tire pressure-monitoring systems for automobiles, battery-charging devices for long-sustainability systems, security or guard systems for homes, and environmental condition-monitoring systems. Figure 8.1 [11] shows a wireless healthcare bio-wireless sensor network (WSN) in a hospital used to monitor the vitals of patients [12]. Each patient wears several sensor nodes in several small monitoring systems, such as an electrocardiogram (ECG). Each system is responsible for specific physiological signals. The central health server can collect the sensed data through wireless communication.

The popularity and widespread use of WSNs may be ascribed to several factors. The first factor is the progress of silicon technology in micrometer and even down to nanometer scales. According to Moore's law [13], the size of transistors on integrated circuits follows a decreasing trend of 0.7× every one and a half years. The gate count on a chip, as well as the operating speed and processing performance, increase significantly. The supply voltage on a silicon chip is also greatly reduced because of thinner oxides in advanced nanometer technologies. Smaller transistors or passive components result in lower parasitic effects and, thus, further reduce power loss. For a scale reduction by factor α ($\alpha > 1$), the power consumption of a shrunk circuit that performs the same task can be reduced by $(1/\alpha)^3$ [1]. The second factor is the progress of RF technology. RF technologies, especially low-power transmission networks such as Zigbee [14] and Bluetooth low energy (BLE) [15], facilitate data transmission and WSN construction. The third factor is the system integration of SoC and a heterogeneous system. A highly integrated SoC greatly decreases the requirements of external components, thereby reducing the volume and weight of the entire system. Heterogeneous integration technologies integrate

Power Management Techniques for Integrated Circuit Design, First Edition. Ke-Horng Chen.

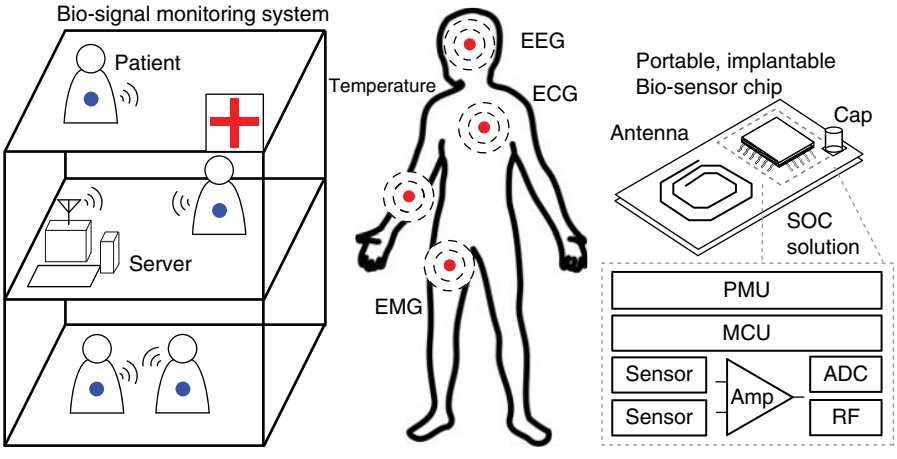

EEG: Electroencephalogram; ECG: Electrocardiogram; EMG: Electromyogram;
PMU: Power management unit; MCU: Micro control unit.

Figure 8.1 Wireless healthcare bio-WSN system

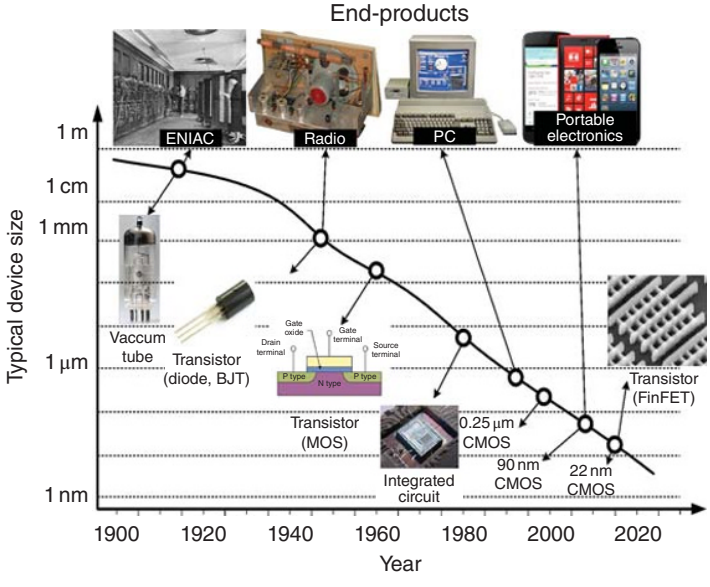

Figure 8.2 Device size reduction through silicon integration technology

micro-electro-mechanical systems (MEMSs), bio-medical or chemical sensors, display devices, and micro-electronic circuits through such technologies as through-silicon via (TSV) and three-dimensional (3D) IC packaging [16]. Consequently, highly integrated systems greatly reduce sensor node size. Figure 8.2 shows the chronological development of size and power reduction because of advanced silicon and system integration technologies.

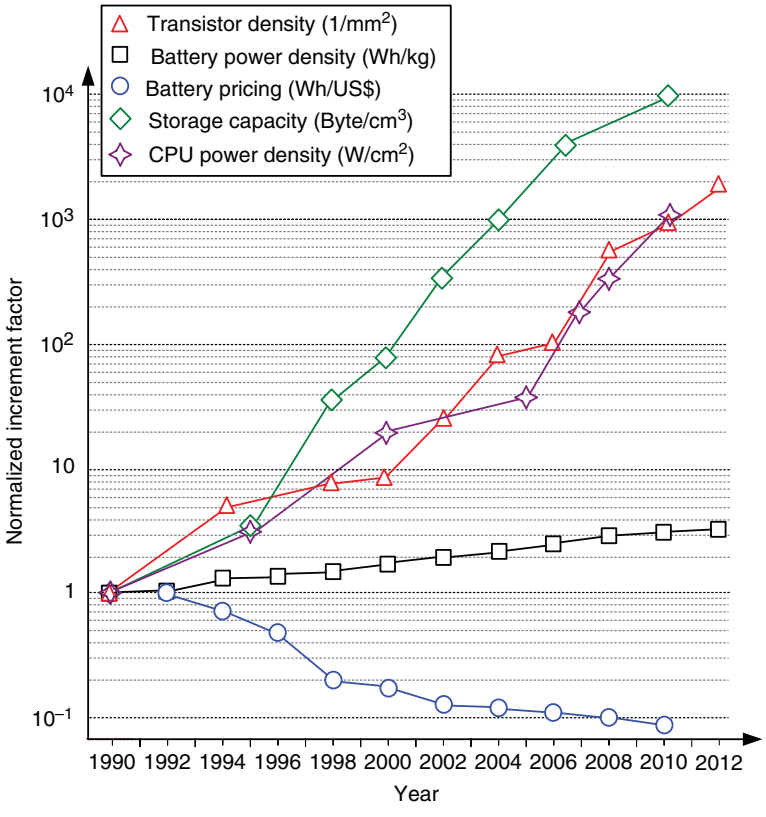

Figure 8.3 Improvement of technologies versus battery energy density

In contrast to rapidly growing silicon and SoC technologies, energy storage technologies do not develop at the same rate, as shown in Figure 8.3 [3]. Developments in battery technologies primarily focus on mass production and packaging, but the materials used in batteries improve slowly. Thus, the prices of batteries drop significantly, but energy density at the same volume increases slowly. Such limitation somehow limits the lifetimes of battery-based portable electronics or sensors.

Technological developments allow low energy consumption, compact size, high performance, and wireless communication in sensor networks or portable electronics. However, operating lifetime remains a challenge. If the quantity and energy density of energy storage devices cannot be improved significantly, the system lifetime can also be prolonged by recharging energy storage devices to allow the system to self-power during normal or standby operation [6–10]. Harvesting energy from the environment is the most suitable choice for the aforementioned demands.

Energy harvesting involves energy source analysis, storage devices, energy conversion circuit design, and material physics [1–9]. Recent developments include components and devices at micro- and macro-scales, encompassing materials, electronics, and integration. The popularity of energy-harvesting technologies has benefited from low-power electronic technology.

Owing to the low-power requirements, low harvested energy in microwatts can be used as energy. Low-power requirements also reduce the size of harvesting source that is capable of generating sufficient energy. An energy-harvesting system has three important components: energy converter (energy source/generator), harvesting circuit, and energy storage device. Energy sources and generators are introduced in Section 8.2. Some specific circuits for different applications are classified and discussed in Section 8.3.

8.2 Energy-Harvesting Sources

As shown in Figure 8.4, the purpose of energy harvesting is to reuse or recycle energy from the environment and artificial facilities or creatures. Energy sources are divided into several types: kinetic energy, thermal energy, and electromagnetic radiation [1, 5].

Kinetic energy is one of the most readily available energy sources from living creatures and the environment. This section provides a brief explanation and the operating principles of conversion of the electrical energy converted from kinetic energy by different transducers. The main principle of kinetic energy harvesting is the displacement of a moving part or the mechanical deformation of a structure. Displacement or deformation can be converted to electrical energy through different methods. Commonly used kinetic energy transducers, namely

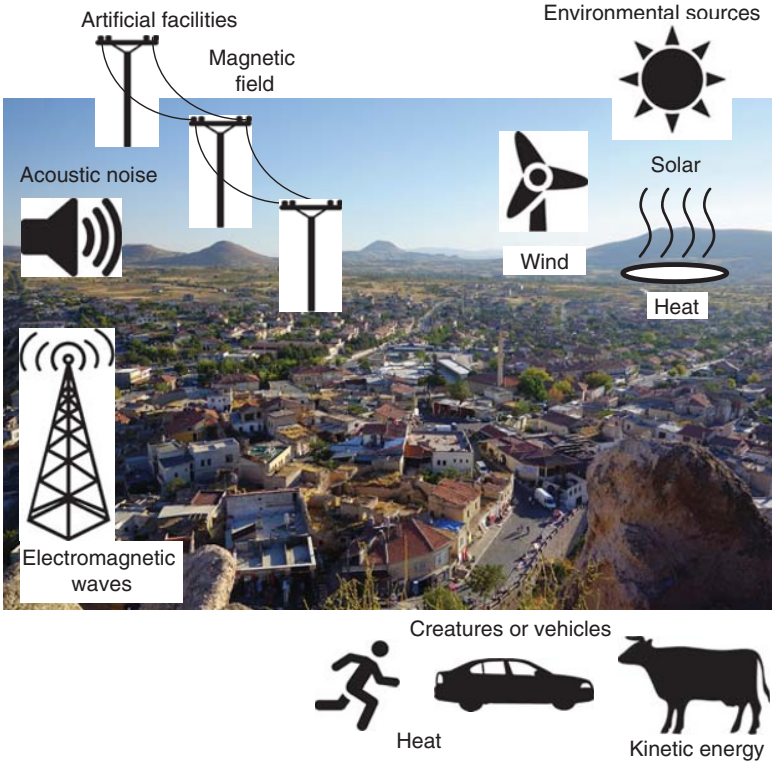

Figure 8.4 Available energy from the environment

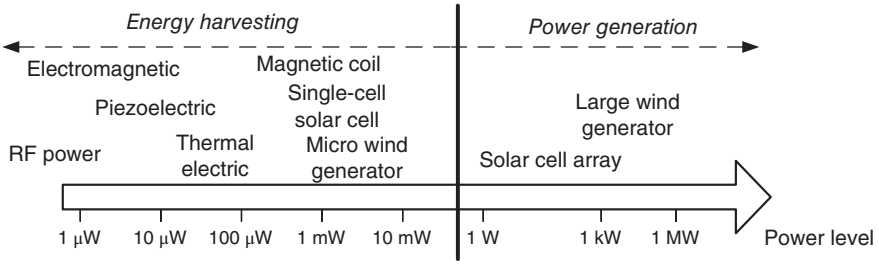

Figure 8.5 Energy scales of various sources

magnetic induction, piezoelectric, and electrostatic transducers, are explained in the succeeding Sections 8.2.1–8.2.3, respectively [1, 5, 17–20]. Wind is also a kinetic energy-induced source obtained from air movement. Wind power transducers, which convert wind power into electrical energy, are introduced in Section 8.2.4 [1, 21–24].

Thermal energy is a widely studied and commercialized energy for low-power electronic devices; thermoelectric systems can generate energy at a scale smaller than 100 μW [1, 5, 25–29]. Thermal energy-harvesting devices can derive thermal energy from different sources, such as humans, animals, machines, and other natural sources. A thermoelectric generator (TEG) basically consists of a thermocouple, which comprises p-type and n-type semiconductors and produces an electrical current proportional to the temperature difference between hot and cold junctions. TEGs are discussed in detail in Section 8.2.5.

Electromagnetic radiation, either in the form of light, magnetic field, or RF microwave, may come from natural or artificial sources. Energy transmission in these sources is wireless and does not necessitate machinery. Solar cell [1,5,30–33], magnetic field [1,5,34], and RF power [1,5,35–38] are discussed in Sections 8.2.6–8.2.8, respectively.

The corresponding energy scales of different energy sources are shown in Figure 8.5. The following subsections introduce eight energy-harvesting transducers of the most commonly harnessed energy sources and describe their respective behaviors. Table 8.1 shows a comparison and the characteristics of different energy sources.

8.2.1 Vibration Electromagnetic Transducers

Vibration occurs in almost all dynamic systems. Electromagnetic transducers are used for harvesting kinetic (vibration) energy. A general model of kinetic energy conversion to electrical power in a vibrating mass is provided in Figure 8.6. This simple equivalent model based on linear system theory was proposed by Williams and Yates [39]; the mathematical description of the model is as follows:

$$M\Delta Z'' + (b_E + b_M)\Delta Z' + K\Delta Z = -M\Delta Y'' \tag{8.1}$$

In Eq. (8.1), M is the weight of the mass, ΔZ is the movement of the mass, ΔY is the input displacement, K is the elasticity coefficient of the spring, b_E is the electrical damping coefficient, b_M is the mechanical damping coefficient, $\Delta Z'$ and $\Delta Z''$ are the first-order and

Table 8.1 Power scales of different sources under given space constraints

	Estimated power (cm^3 or cm^2)	Output type	Output range
Solar cell	**10 μW to 15 mW** (Outdoors: 0.15–15 mW) (Indoors: <10 μW)	DC	1 V (single cell)
Kinetic energy	**<1–200 μW** (Piezoelectric: ~200 μW) (Electrostatic: 50–100 μW) (Electromagnetic: <1 μW)	AC	Tens of volts (peak voltage)
Thermal	**15 μW** (10°C gradient)	DC	10–100 mV
RF power	**<1–300 μW** (Source dependent)	AC	Hundreds of microvolts
Wind power generator	**<10–1000 μW**	AC	Generator dependent several volts, that is, approximately tens of volts
Magnetic coil	N/A	AC	Coil dependent several volts, that is, approximately tens of volts

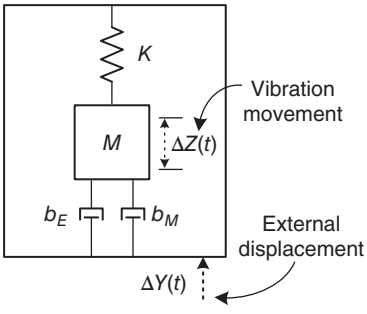

Figure 8.6 Schematic of a generic vibration converter

second-order differential results of ΔZ, respectively. $\Delta Z'$ and $\Delta Z''$ represent the velocity and the acceleration of the mass, respectively. $\Delta Y''$ represents the acceleration of the input displacement. The model is based on force balance. The energy transferred from the oscillating mass and converted to electricity behaves like a linear damper to the mass spring system. The kinetic power converted to electricity in the system is equal to the decreased power from mechanical vibration. The electrically induced force is $b_E \Delta Z$. Power can be defined as the product of force and velocity. For example, with the integration of force $b_E \Delta Z$ and velocity $\Delta Z'$ by Laplace transform and mathematical derivation, the magnitude of the output power can be defined as in Eq. (8.2). In this equation, ζ_T is the combined damping ratio of ζ_E and ζ_M (where ζ_E is the equivalent electrical damping ratio and ζ_M is the equivalent mechanical damping ratio); A is the acceleration magnitude of input vibrations, and ω is the frequency of the driving vibration [17,18].

$$|P| = \frac{M\zeta_E A^2}{4\omega\zeta_T^2}, \text{ where } \zeta_T = \zeta_E + \zeta_M \tag{8.2}$$

Equation (8.2) shows the relationship of mass and the acceleration magnitude and frequency of vibration. As shown in Eq. (8.2), a higher mass and a higher acceleration have more output power. Owing to the nature of vibration, a higher vibration frequency results in a decreased acceleration if the spring of a damping system similar to the system illustrated in Figure 8.6 has constant elasticity coefficient K, This premise suggests that the transducer should be designed to resonate at the lowest fundamental frequency in the input spectrum rather than at higher harmonics. The loss in the mechanical structure is denoted by ζ_M and should be as low as possible. Finally, the amount of power is linearly proportional to the mass. Thus, the converter design should allow for the largest possible mass within the space constraints.

By using input vibrations and applying Faraday's law, electromagnetic power conversion is obtained from the relative motion of an electrical conductor in a magnetic field. According to Faraday's law, the variation in a magnetic flux through an electrical circuit creates an electric field. This flux variation can be realized with a moving magnet, wherein the flux is linked with a fixed coil or with a fixed magnet with a flux linked to a moving coil. The first configuration is preferred to the second one because the electrical wires are fixed. A simple example of a linear electromagnetic generator is shown in Figure 8.7 [8,40,41].

The voltage on the coil is determined by Faraday's law, as expressed in Eq. (8.3), where ε is the induced electromagnetic field and Φ_B is the magnetic flux:

$$\varepsilon = -\frac{d\Phi_B}{dt} \tag{8.3}$$

The open-circuit voltage V_{Out}, which is generated by the linear electromagnetic generator, is defined by Eq. (8.4), where N is the number of turns in the coil, B is the magnetic strength of the magnet, A_{Coil} is the cross-sectional area of the coil, and v is the velocity of the magnet as it travels through the coil. If the generator is loaded with resistance, power is extracted from the generator and a current will flow in the coil. This current creates its own magnetic field, which opposes the field inducing it. The interaction between the field caused by the induced current and the field from the magnets produces a force that opposes the motion.

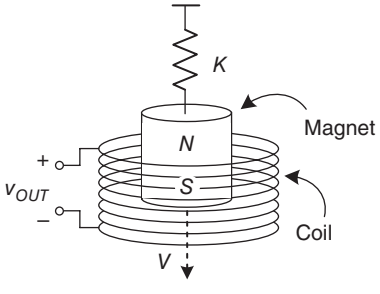

Figure 8.7 Electromagnetic generator

$$V_{Out} = NBA_{Coil}v \tag{8.4}$$

The output voltages of electromagnetic transducers are low, in the range of 100 mV. The main drawback of electromagnetic transducers is their difficulty to be integrated into electronic and micro systems. Low energy density also limits the application of electromagnetic transducers.

8.2.2 *Piezoelectric Generator*

In 1880, the Curie brothers discovered the piezoelectric effect in quartz crystals. Generally, the piezoelectric effect can be defined as the conversion of mechanical energy into electrical energy (direct effect) or the conversion of electrical energy into mechanical energy (inverse effect). Certain materials suffer from electrical polarization proportional to the applied strain when subjected to mechanical strain. Figure 8.8 shows a schematic of a piezoelectric cantilever [1,3,5].

The constitutive equations for a piezoelectric material are given in Eqs. (8.5) and (8.6), where δ is the mechanical strain, σ is the mechanical stress, Y is the modulus of elasticity [3], d is the piezoelectric strain coefficient, D is the electrical displacement (charge density), E represents the electric field, and ε_P is the dielectric constant of the piezoelectric material:

$$\delta = \frac{\sigma}{Y} + dE \tag{8.5}$$

$$D = \varepsilon_P E + d\sigma \tag{8.6}$$

Equation (8.5) is a combination of Hooke's law, represented by the term dE, and the piezoelectric coupling, denoted by the term σ/Y. Similarly, Eq. (8.6) is a combination of Gauss's law for electricity, represented by the term $\varepsilon_P E$, and the piezoelectric coupling, denoted by $d\sigma$. Piezoelectric coupling provides a two-way conversion between mechanical energy and electrical energy. The electric field across the material affects its mechanics, whereas stress in the material affects its dielectric properties.

Piezoelectric devices are commonly assumed to provide high voltages and low currents. However, voltage and current levels depend on the physical implementation and the particular

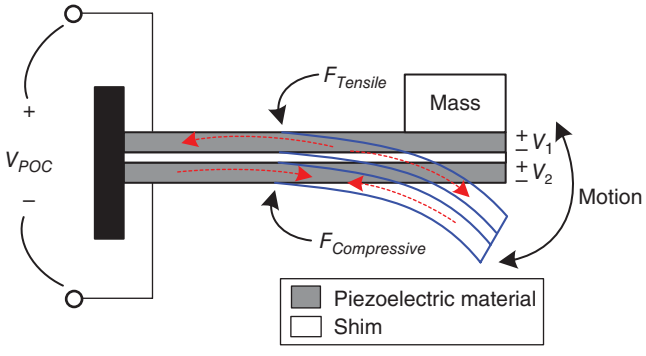

Figure 8.8 Schematic of a piezoelectric cantilever

electrical load circuit used. In reality, designing a system that produces voltages and currents in a useful range is fairly easy. Experimental results show that a conversion voltage in the range of several volts and a conversion current on the order of tens to hundreds of microamperes are achievable. The advantage of piezoelectric conversion is the direct generation of appropriate voltages. Owing to the high energy density, piezoelectric generators are considered to be a relatively good option for vibration energy harvesting compared with electromagnetic and electrostatic energy generators.

8.2.3 *Electrostatic Energy Generator*

The working principle of electrostatic generators indicates that the moving part of the transducer moves against an electrical field, thus generating energy [1,3,5]. A rectangular parallel plate capacitor is used to illustrate the principle of electrostatic energy conversion. The voltage V across the capacitor is expressed by Eq. (8.7), where Q is the charge on the capacitor, d is the gap or distance between plates, A is the area of the plate, and ε_0 is the dielectric constant of the free space. Figure 8.9 shows a schematic of an electrostatic generator.

$$V = \frac{Qd}{\varepsilon_0 A} \tag{8.7}$$

The capacitance is defined by:

$$\frac{Q}{V} = C = \frac{\varepsilon_0 A}{d} \tag{8.8}$$

If the charge on the plates is held constant, the voltage can be increased by reducing the capacitance. A voltage increase by capacitance reduction can be achieved either by increasing the distance d between plates or by reducing A. The energy stored in the capacitor is expressed by Eq. (8.9). If the voltage is held constant, the charge can be increased either by reducing d or increasing A. Increasing the voltage or charge increases the energy stored in the capacitor. Thus, energy transfer schemes can be classified as either charge- or voltage-constrained conversion; both energy transfer schemes are adopted in various works [1].

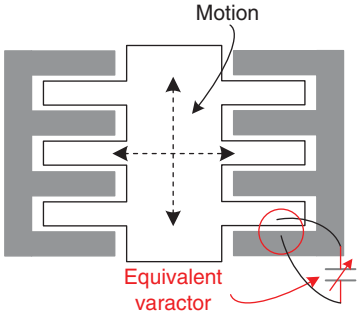

Figure 8.9 Schematic of electrostatic generator

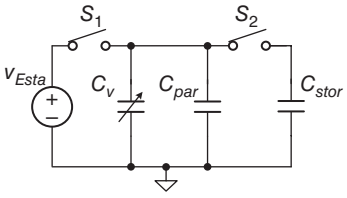

Figure 8.10 Electrostatic conversion circuit model

$$E_{stat} = \frac{1}{2}QV = \frac{1}{2}CV^2 = \frac{Q^2}{2C} \tag{8.9}$$

The main disadvantage of electrostatic generators is the voltage source requirement to initiate the conversion process because the capacitor must be charged to an initial voltage. Figure 8.10 shows an example of an electrostatic conversion circuit [42]. A V_{Esta} voltage source is used as the supply source to charge the equivalent varactor C_V. The maximum voltage $V_{CV,max}$ on the varactor according to the capacitance difference in each vibration is shown in Eq. (8.10), where C_{max} and C_{min} are the maximum and minimum capacitances of the varactor C_V, respectively, and C_{par} is the parasitic capacitance of C_V:

$$V_{CV,max} = V_{Esta} \cdot \frac{(C_{max} + C_{par})}{(C_{min} - C_{par})} \tag{8.10}$$

In each vibration cycle, the energy generated by the electrostatic generator E_{stat} is shown as:

$$E_{stat} = \frac{1}{2}{V_{Esta}}^2 \cdot (C_{max} - C_{min}) \cdot \left(\frac{C_{max} + C_{par}}{C_{min} + C_{par}}\right) = \frac{1}{2}V_{CV,max} \cdot V_{Esta} \cdot (C_{max} - C_{min}) \tag{8.11}$$

C_{max} and C_{min} can vary from hundreds to several pico-farads. The considerable difference between C_{max} and C_{min} results in a large variation in $V_{CV,max}$. Such a variation could reach hundreds of volts at a 1 V supply of V_{Esta}. The high output voltage places a constraint on device selection. An additional disadvantage of electrostatic generators is the possibility of the capacitor plates coming into contact with each other suddenly, thereby resulting in a short circuit. Thus, mechanical stops must be included in the design. Despite its limitations, electrostatic generators can still be considered a good option for SoC applications because of their potential to be integrated into silicon processes through MEMs technology.

8.2.4 Wind-Powered Energy Generator

For decades, wind generators (WGs) have been a well-known renewable energy source utilized in large-scale electric power generation in grid-connected applications. In recent years, micro-WGs, as shown in Figure 8.11, have been used as energy-harvesting sources for indoor or autonomous monitoring systems as these power sources become more popular [1,21–24]. Despite the demand for growth in harvesting, not all locations have strong winds. Thus, the challenge in designing a micro-WG is to make it work even at low wind speeds.

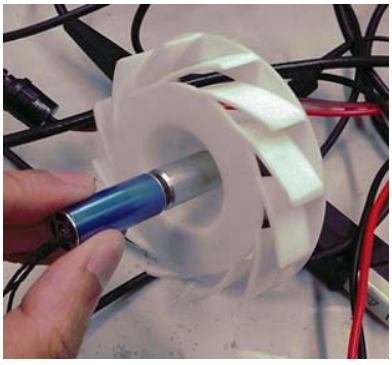

Figure 8.11 Micro-wind generator

The harvested power P_{WT} captured by a wind turbine is related to blade shape, pitch angle, and radius speed. Equation (8.12) defines P_{WT} and shows the related parameters. In Eq. (8.12), ρ is air density (typically 1.25 kg/m^3); $T_p(\lambda, \beta)$ is the wind-turbine power transfer function, which varies with the design; β is the pitch angle (degrees); λ is the tip-speed ratio; R is the blade radius (m); and V is the wind speed (m/s).

$$P_{WT} = \frac{1}{2}\pi\rho T_p(\lambda,\beta)R^2V^3 \tag{8.12}$$

In Eq. (8.12), the coefficient of T_p is limited to 0.59 according to the Betz limit [23]. The tip-speed ratio λ in Eq. (8.13) is the ratio between the rotational speed of the tip of a blade and the actual velocity of the wind, V, where Ω is the WG rotor speed of rotation (rad/s).

$$\lambda = \frac{\Omega R}{V} \tag{8.13}$$

Wind turbines convert the kinetic energy of the generated wind because the principle of wind power is the same as that of normal electricity generation. By multiplexing the efficiency of the generator, η_G, the total power, P_{WG}, produced by the WG is given as:

$$P_{WG} = \eta_G P_{WT} \tag{8.14}$$

The WG power coefficient is not constant but maximized for a tip-speed ratio $\lambda_{optimal}$. A specific point exists at which the WG output power is maximum at a certain rotation speed. The WG power curves at various wind speeds are shown in Figure 8.12 [21]. Figure 8.12 shows that the value of the optimal tip-speed ratio is constant for all maximum power points (MPPs). As shown in Eq. (8.15), the speed of WG rotation is related to wind speed, where Ω_n is the optimal rotation speed at a certain wind velocity V_n:

$$\Omega_n = \lambda_{optimal}\frac{V_n}{R} \tag{8.15}$$

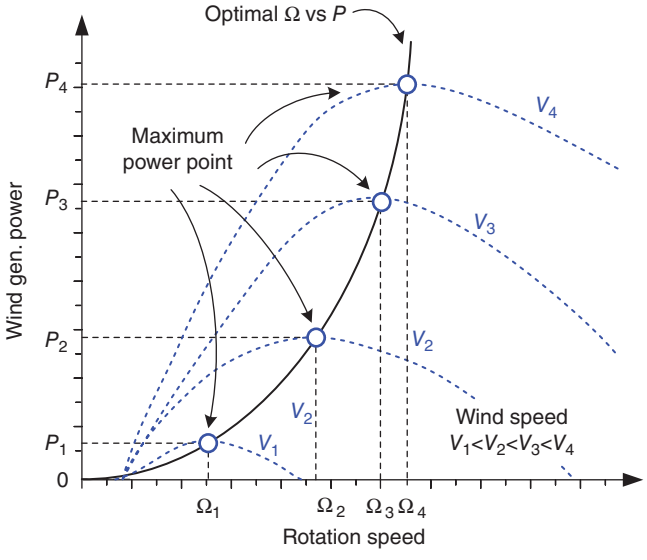

Figure 8.12 Rotation speed vs. generated power

Different rotation speeds at the same wind speed result in different generated powers. The loading condition influences the operating speed of a WG because the current generated by the generator produces a torque that is the inverse of the torque of the wind turbine. The balance between the input torque and the inverse torque can be achieved through load control to extract maximum power. Wind power depends on environmental conditions. Micro-WGs can generate several milliwatts of power, which is relatively large in the scope of energy harvesting. Through continuous harvesting, the power generated by a micro-WG is capable of fully meeting the power requirement of a monitor sensor. However, the drawback of wind power is the large size of WGs. Reducing the size of WGs is difficult because of the wind power density and wind turbine mechanism. Wind power is considered a competitive option for monitoring environmental factors.

8.2.5 Thermoelectric Generator

The thermoelectric effect is the direct conversion of temperature differences to electric voltage and vice versa. A thermoelectric device produces voltage when the temperature on one side is different from that on the other side. Conversely, when a voltage is applied to a device, a temperature difference is generated [1,5].

Thomas Johann Seebeck discovered that a compass needle was deflected by a closed loop formed by two metals in which a temperature difference existed in the junctions. This effect is attributed to the metals responding differently to the temperature difference, creating a current loop and a magnetic field. Seebeck did not realize that the magnetic field was induced by an electric current. This phenomenon was called the thermomagnetic effect until Danish physicist Hans Christian Ørsted corrected the mistake and renamed the phenomenon "thermoelectricity."

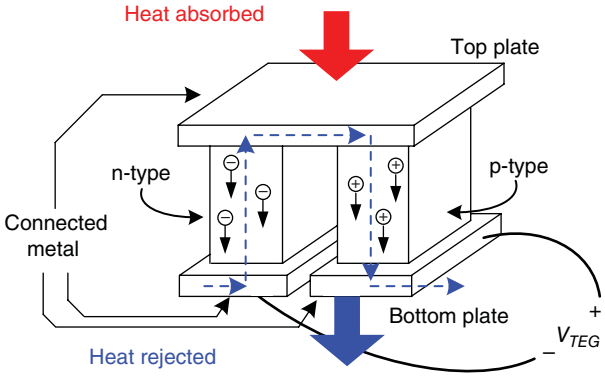

Figure 8.13 Schematic of a thermoelectric generator

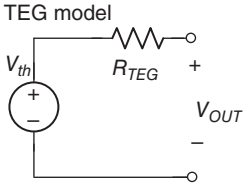

Figure 8.14 Model of a thermoelectric generator

Following developments in the study of thermoelectricity, current thermoelectric generators (hereafter TEGs) are currently solid-state devices. Figure 8.13 shows a schematic of a TEG. Charge carriers in metals and semiconductors are free to move, and resemble gas molecules that carry charge and heat. When a temperature gradient exists in a material, the mobile charge carriers at the hot end preferentially diffuse to the cold end. The collection of charge carriers results in a net charge and an electrostatic potential buildup. This mechanism is the basis of thermoelectric power generation.

Figure 8.13 shows a semiconductor thermoelectric couple, or a thermocouple consisting of n-type (containing free electrons) and p-type (containing free holes) thermoelectric elements [25–29]. The electron and hole carriers flow in opposite directions and therefore constitute a net current. The best thermoelectric materials are heavily doped semiconductors. The output voltage of TEGs is in the range of several millivolts, and to achieve reasonable output voltages a large number of thermocouples are required. These thermocouples are placed electrically in series and thermally in parallel. Figure 8.14 shows an equivalent model of a TEG, wherein V_{th} represents the voltage generated by the TEG and R_{TEG} is the inner resistance of the TEG.

The temperature difference generates a voltage V_{TEG} as defined in Eq. (8.16), where α is the Seebeck coefficient and ΔT is the temperature difference from the top plate to the bottom plate. V_{TEG} is the open-circuit voltage generated in the TEG. Heat flow drives the electrical current, which also determines the power output:

$$V_{TEG} = \alpha \Delta T \tag{8.16}$$

According to Carnot's theorem [1], the energy transfer between heat reservoirs has a limited efficiency, which is defined by Eq. (8.17). This limiting value, η_{th}, is called the Carnot cycle efficiency because it is the ideal efficiency. T_h and T_c are the temperatures on the top plate and the bottom plate, respectively:

$$\eta_{th} = 1 - \frac{T_c}{T_h} \tag{8.17}$$

TEG converts heat (Q) into electrical power (P) at efficiency η:

$$P = \eta Q \tag{8.18}$$

Efficiency η is not a constant value because it varies with the temperature difference $T_h - T_c$ between thermoelectric plates. The efficiency of a TEG increases nearly linearly with temperature difference. This effect is due to the characteristic of TEGs and all heat engines, that is, efficiency is limited by the Carnot cycle. Equation (8.19) briefly describes the efficiency of TEGs, where η_r is the reduced efficiency, the efficiency relative to the Carnot efficiency:

$$\eta = \Delta T \frac{\eta_r}{T_h} \tag{8.19}$$

The energy transmission efficiencies of TEGs are often lower than 10%. The rejected heat must be removed through a heat sink, which requires an additional heat-dissipation mechanism and a larger area. TEGs are silent, reliable, and scalable. They are extremely suitable for small distributed power generation in energy-harvesting applications, such as bio-WSNs.

8.2.6 Solar Cells

Solar energy generation or photovoltaics (PVs) are a method of generating electrical power by converting solar radiation directly into electricity using semiconductors that exhibit the PV effect [1,5]. Solar energy generators are a mature technology for large-scale energy generation. PV systems generate energy in milliwatts to megawatts. The generated electricity can be used for numerous applications, such as water heaters, signal lamps, and grid-connected PV systems, as shown in Figure 8.15 [43]. The application of PVs in portable products, such as calculators, watches, or monitoring sensor nodes, is a valid option under appropriate conditions.

In an outdoor environment on a sunny midday, the power density of the solar radiation on the earth's surface is about 100 mW/cm^3, which is approximately three times as high as that of other harvesting sources. However, solar energy is not particularly attractive for indoor environments because the power density drops to as low as 10–20 μW/cm^3. Silicon solar cells are a mature technology that can be divided into two major types: single-crystal silicon and thin-film polycrystalline. The efficiency of single-crystal silicon cells ranges from 12 to 25%. Thin-film polycrystalline and amorphous silicon solar cells are also commercially available and have lower cost and efficiency than single-crystal silicon cells. Table 8.2 shows the output power under various conditions of a single-crystal silicon solar cell with 15% efficiency. The power density of solar radiation decreases approximately as $1/d^2$, as expected, where d is the distance from the light source.

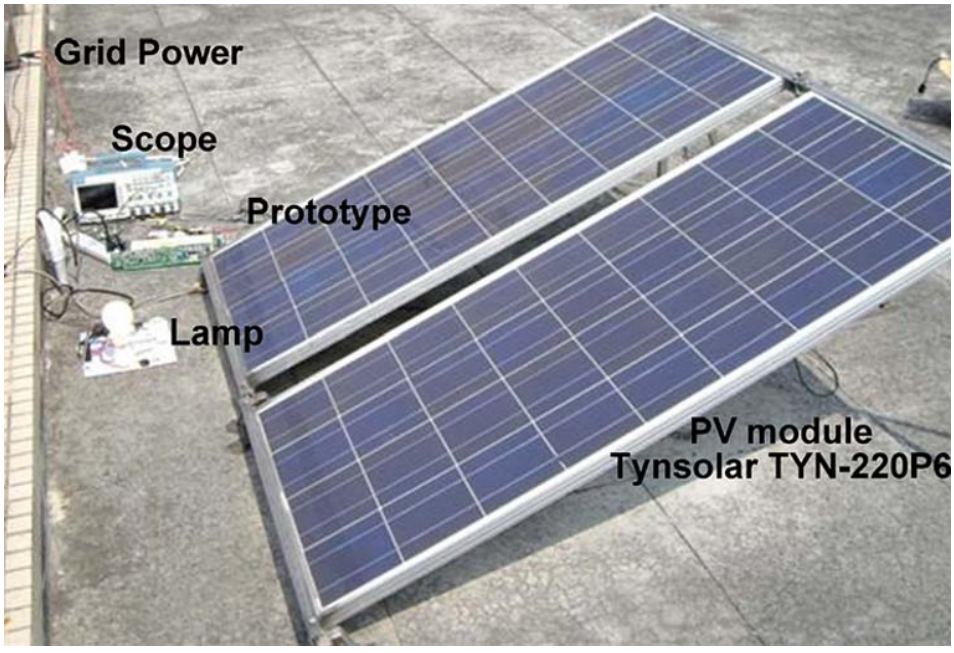

Figure 8.15 Outdoor solar cell

Table 8.2 Solar cell power under various conditions

Conditions	Outdoor, midday	Outdoor, overcast	10 cm from 60 W bulb	38 cm from 60 W bulb	Indoor lighting
Power ($\mu W/cm^3$)	15 000	750	5000	550	6.5

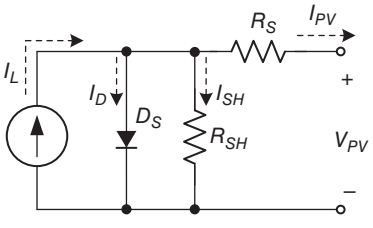

Figure 8.16 Modeling of a solar cell

A model of a solar cell is provided in Figure 8.16 [30–33]. Two parasitic resistances, that is, a parallel shunt resistance R_{SH} and a series resistance R_S, and a parallel diode are included in this model. The output current of the PV cell, I_{PV}, is expressed as in Eq. (8.20), where I_L represents the current generated by the solar cell, I_D represents the voltage-dependent diode current, and I_{SH} represents the current lost due to shunt resistances. The diode current I_D is modeled using the Shockley equation for an ideal diode, where n is the diode ideality factor (normally between 1 and 2 for a single-junction cell), I_0 is the saturation current, V_T is the thermal voltage, k is Boltzmann's

constant (1.381×10^{-23} J/K), and q is the elementary charge. For an ideal cell, R_{SH} is infinite and provides no current leakage, whereas R_S is zero. No voltage drop was observed in V_{PV}:

$$I_{PV} = I_L - I_D - I_{SH} = I_L - I_0\left(e^{\frac{q(V_{PV}+I_{PV}R_S)}{nkT}} - 1\right) - \frac{V_{PV}+I_{PV}R_S}{R_{SH}} \tag{8.20}$$

The current generated by solar cells during operation is shared by the power losses in internal resistances and diodes. The characteristic curves of solar cell panels, which include the different irradiation levels and different ambient temperatures, are shown in Figure 8.17. In Eq. (8.21), the open-circuit voltage, V_{OC}, and the short-circuit current, I_{SC}, multiplied by the fill factor, FF_N, represent the efficiency of cell η. The power is zero at I_{SC} and V_{OC}. The voltage and current at the MPP are denoted by V_{MP} and I_{MP}, respectively. P_{in} represents the input irradiation power. As shown in Eq. (8.22), FF_N is defined as the ratio of the realistic MPP $P_{max,n}$ and the theoretical power $P_{T,n}$, which is the product of I_{SC} and V_{OC}:

$$\eta = \frac{I_{SCN} \cdot V_{OCN} \cdot FF_N}{P_{in}} \tag{8.21}$$

$$FF_N = \frac{P_{max,n}}{P_{T,n}} = \frac{I_{MPN} \cdot V_{MPN}}{I_{SCN} \cdot V_{OCN}} \tag{8.22}$$

The maximum available power provided by the solar cell, P_{max}, is related to the ambient temperature and irradiation level, as shown in Figures 8.17 and 8.18 [43]. Given their high energy density, PV cells are a good choice of energy source in places with sufficient light. However, the output power of PV panels varies significantly with the output voltage and current. Thus, commercial PV inverter products usually use a maximum power point tracking (MPPT) technique to achieve superior energy extraction from PV panels.

8.2.7 *Magnetic Coil*

Electromagnetic transducers use kinetic energy to induce magnetic-field-flux variation on a fixed coil to generate energy. Aside from the moving magnet, the alternating current on a power

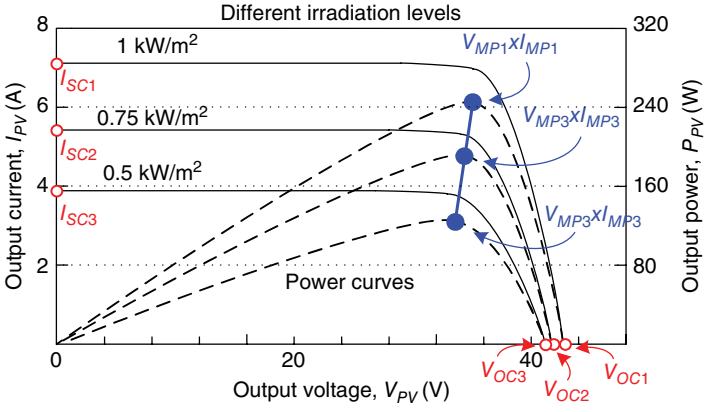

Figure 8.17 Characteristic curves of a solar panel at different irradiation levels

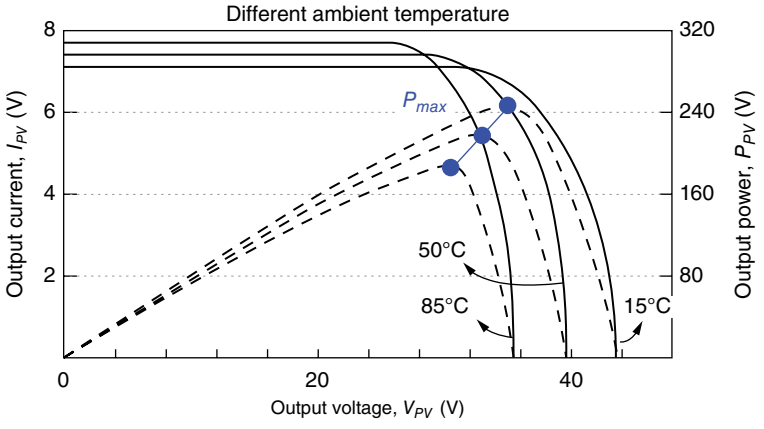

Figure 8.18 Characteristic curves of a solar panel at different temperatures

line also generates a time-variant magnetic field. The magnitude of the magnetic field variation is proportional to the current on the power wire; a large current with a large magnetic flux can generate considerable energy [1,5].

Current sensors, such as a Rogowski coil and current transformers (CTs), which are based on Faraday's law of induction, are conventionally used to provide inherent electrical isolation between the output signal and the current measured [34]. Figure 8.19 shows a schematic of a Rogowski coil, where r is the radius of the coil and V_{Rcoil} is the open-circuit voltage. The path integral of magnetic flux density B inside the coil is expressed as in Eq. (8.23), where μ_0 is the permeability of the free space and I_{AC} is the current in the power wire. Current I_{AC} flows through an enclosed area surrounded by a curve denoted by C:

$$\oint_C \vec{B} \cdot d\vec{l} = \mu_0 I_{AC} \tag{8.23}$$

If the cross-sectional diameter of the Rogowski coil is smaller than its radius r, then the magnetic flux density B can be simplified as:

$$B = \frac{\mu_0 I_{AC}}{2\pi r} \tag{8.24}$$

By applying Faraday's law of induction, the output voltage of the Rogowski coil undergoing a change in current I_{AC} can be obtained using Eq. (8.25). A is the cross-sectional area of the coil body, which is formed by the windings, k is the integration constant, and N is the number of turns. Voltage V_{Rcoil} is proportional to the derivative of I_{AC} plus the initial voltage $V_{Rcoil}(0)$:

$$V_{Rcoil} = -N\frac{d\phi}{dt} = \frac{\mu_0 NA}{2\pi r} \cdot k \int_t \frac{dI_{AC}}{dt} \cdot dt + V_{Rcoil}(0) = \frac{-\mu_0 NA}{2\pi r} \cdot k \cdot I_{AC} + V_{Rcoil}(0) \tag{8.25}$$

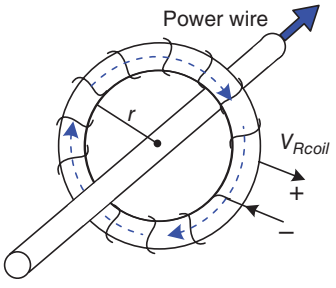

Figure 8.19 Schematic of a Rogowski coil

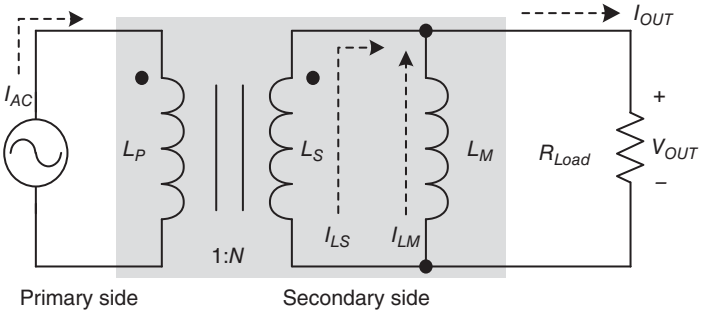

Figure 8.20 Model of a CT

CTs, which also utilize Faraday's law of induction to measure currents, are similar to a Rogowski coil. The construction of a CT is basically the same as that of a Rogowski coil, but a core material with high relative permeability is inserted into the former. The output of a Rogowski coil is a voltage that is proportional to the derivative of the primary current. The output of a CT is a sensing current on secondary winding, I_{Out}. Thus, the output of a CT is loaded with a sense resistor, R_{Load}. The current through R_{Load} generates a magnetic flux that counters the flux generated by the primary current. The CT model with sense resistor R_{Load} depicted in Figure 8.20 [34] neglects stray inductances, core losses, and winding resistances. However, such a CT can still provide sufficient insight into the CT operation principle. Figure 8.20 shows that I_{AC} represents the sensing current from the appliance. L_P is the primary-side inductance, L_S is the inductance induced by the primary side, and L_M is the magnetizing inductance. Thus, I_{LM} is influenced by the voltage across L_M and I_{LS} is induced by I_{AC}; I_{Out} can be expressed as the summation of I_{LM} and I_{LS}:

$$I_{Out} = I_{LS} + I_{LM} = \frac{I_{AC}}{N} - \frac{1}{L_M}\int_t V_{Out} \cdot dt \tag{8.26}$$

In current sensing, R_{Load} should be very low to reduce the current I_{LM} and enhance the sensing accuracy. By contrast, the most important issue in energy-harvesting applications is the transfer of maximum energy from a CT. The loaded resistor should match the equivalent resistor of a CT to extract the maximum power. Monitor sensors placed on the power lines of an electrical appliance can use a CT as power source.

8.2.8 RF/Wireless

The concept of wireless energy transmission is not new. Approximately 100 years ago, Nikola Tesla attempted to transmit low-frequency energy over long distances. In the 1950s, the rectification of microwave signals was proposed and researched in the context of high-power beaming. Figure 8.21 shows an experiment on wireless power transmission [44]. Near-field wireless energy transmission is omnipresent. All passive radio frequency identification (RFID) tags function on the same principle.

Wireless power transmissions can be classified into two categories: near field and far field [1,5,35–38]. These are the regions of the electromagnetic field around a radiation-emitting object, such as a transmitting antenna. Near field is normally within a distance of a few wavelengths. The distance beyond the near field is called the far field. The near field produces electromagnetic induction and electric charge effects on the electromagnetic field. A near-field transmission involves energy transfer effects that couple directly to the receivers near the antenna. Thus, a near-field transmission functions like a transformer, which draws more power at the primary circuit if power is drawn from the secondary circuit. By contrast, a far-field transmission constantly draws the same energy from the transmitter regardless of the receiving condition at the receiving part.

However, energy-harvesting applications collect ambient energy from the environment. The principle of near-field transmission, which consumes more power for transmitters, is related more to power transmitting than power harvesting. Thus, RF-harvesting applications are mainly focused on far-field transmission. Numerous potential RF sources, such as broadcast radio, mobile telephony, and wireless networks, exist in populated areas.

Equation (8.27) shows the difference between the received power versus the transmitted power. In Eq. (8.27), P_{rad} is the power incident on the node, P_S is the radiative power, λ is the wavelength, and R is the distance between the reader and the node:

$$P_{rad} = \frac{P_S \lambda^2}{4\pi R^2} \tag{8.27}$$

The available power decreases rapidly with an increase in propagation distance. In reality, the transmitted power drops quickly at a rate faster than $1/R^2$ in an indoor environment. A more

Figure 8.21 RF power transmission: MIT demonstration first showed how electricity can be wirelessly transferred to a device

likely figure is $1/R^4$ [35–38]. The target of RF energy harvesting is to collect as much RF as possible from disparate sources and convert the collected RF into useful energy. Energy collection is based on the antenna. However, a few challenges to far-field transmission exist. First, the received energy is very low, only on the nano-watt scale. Both high radiation frequency and the passive circuit structure of most RF-harvesting circuits are detrimental to efficiency. A high input frequency hinders utilization of the active circuit to enhance efficiency, and the power consumption of a high-speed control circuit is correspondingly high. Second, energy collection is achieved by the antenna. Each antenna has its own characteristic impedance and matching frequency. Thus, harvesting multiple frequencies from different sources with the use of a single antenna is difficult. The energy levels presented by RF energy sources are too low to fully provide all requirements of present electronic devices.

8.3 Energy-Harvesting Circuits

8.3.1 Basic Concept of Energy-Harvesting Circuits

Energy-harvesting transducers transfer energy from the sources described in Section 8.2. These sources are environmentally dependent, and the intensities of light, heat, magnetic field, and vibration are neither constant nor predictable. To extend the sustainability of a system, one should observe the level of the available energy and balance it with the power consumption of the system. Environmental characteristics define the possible energy-harvesting source. After the selection of the energy-harvesting source through the appropriate selection of a power converter topology, the harvested energy can be used efficiently [1–9,25,30].

In conventional portable electronics as well as in sensor nodes, batteries are the most commonly used power source as they are the most cost-effective choice. Aside from cost, batteries have the advantages of widespread availability, high reliability, mature mass-produced technology, minimal to zero environmental calibration requirement, ease of use (no need for thermal, vibrational, or photonic exposure beyond the sensor goals), and less energy-conversion overhead (the battery is the voltage source). However, battery replacement is a major issue for some sensing applications. Sometimes, battery volume may induce a problem when the sensor nodes have volume constraints.

Despite the power dissipation of circuits, a battery self-discharges by 0.1–5% per month because of its chemistry. The self-discharge rate depends on the material of the battery. High-temperature exposure tends to increase the self-discharge rate of batteries. Regardless of the cost, the suitability of an application for environmental energy harvesting is determined based on two factors: lifetime and environment. The lifetime of a system with a battery supply (under certain size limitations) can be estimated. System lifetime can be considered a benchmark for the lifetime of a harvesting supply. Environmental conditions define the available power and decide what kind of energy source should be harnessed. Considering the use of an energy-harvesting system, the overall performance needs to outperform a battery solution in terms of energy density, power density, and/or cost. Typically, the niche for energy harvesting is in long-lived applications in which the energy density is critical; the location of the sensor nodes may not be reachable and the replacement operations may be too numerous to perform [1].

In recent years, the application of energy-harvesting systems has focused mainly on WSNs. To define a power supply structure, the power requirement of a sensor node in a WSN, as

shown in Figure 8.22 [3,4], should be analyzed. The power demands of the sensor nodes may therefore be raised to five or six orders, from 100 nW (e.g., 1 V and 100 nA of load power) during the sleeping mode to over 100 mW during the RF-transmitting mode. Under the variable conditions listed in Table 8.3, the limited and unstable environmental energy can hardly offset

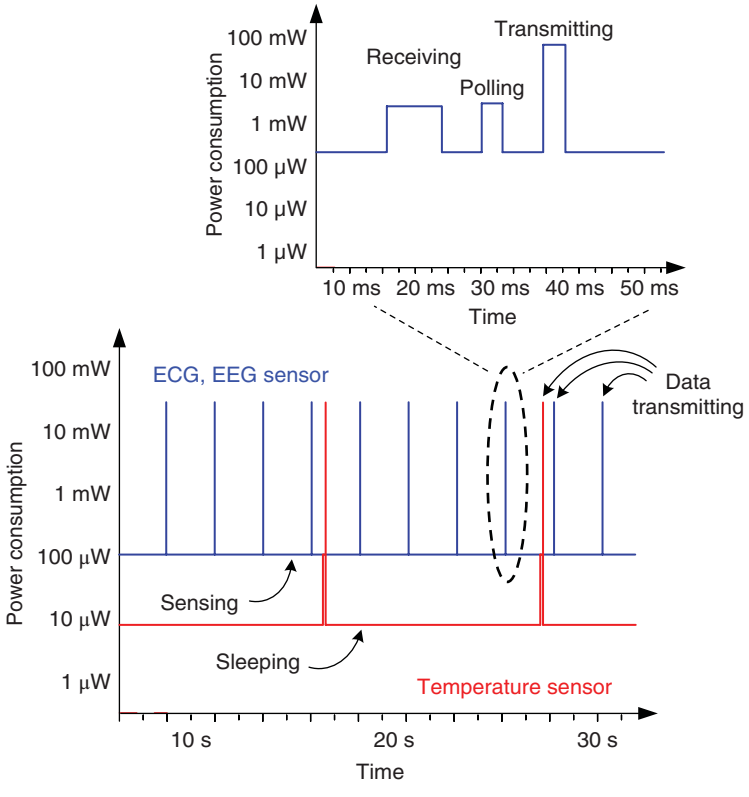

Figure 8.22 Power status of wireless sensor nodes

Table 8.3 Power status and operating mode of wireless sensor nodes

	Power consumption	Period (s)	Demand
Sleeping	10^{-1}–10^{2} μW	10^{-1}–10^{4}	The minimum power to enable the circuit to wake up when events occur
Sensing	10 μW–10 mW	10^{-4}–10^{4}	Readout, conversion, and storage signals from the sensor
Receiving	10^{-1}–10 mW	10^{-3}–1	Listening to data packets or commands from the server
Polling	10 μW–10^{2} mW	10^{-5}–10	Signal processing, which may be combined with sensing circuit operation
Transmitting	1–10^{2} mW	10^{-6}–1	Sending of status, data, or command to the server

the power consumption of the sensor nodes. In fact, the output power of state-of-the-art harvesting technologies is not yet commensurate with high-power-consuming loads, such as in the case of power amplifiers and their associated antennae. The propagated energy of the RF communication signal decreases by the square of the distance traveled. The power requirement of PAs unavoidably increases as the telecommunication distance increases.

From the information in Table 8.3 and the characteristics of WSNs, if the sensor nodes rely only on the harvested energy, then two problems may be encountered. First, the harvested energy may not be sufficient to supply the dynamic system loading. The average power derived from the harvesting source may be higher than the average power requirement of the sensor node, but the large transient power requirement is not affordable. Second, even if the harvested energy is sufficient for the dynamic system loading, a storage device is still needed for the high efficiency demand. Energy efficiency, which is related to the MPPT, will be described in Section 8.4.

A hybrid-mode power supply system is recommended to overcome the disadvantages of an energy-harvested and battery-supplied system. The use of a rechargeable battery is a preferred method for the harvested energy. The battery supplies high power (up to several milli-watts) during a short period of time (during the receiving, transmitting, and polling modes). For the rest of the time, the energy harvester charges the battery with a trickle current. Figure 8.23 shows a system diagram of a conventional serial harvesting system. The AC/DC to DC/DC converter stage deals with the input source and generates a charging current for the storage device. The DC/DC converter stage performs a regulation function. This structure conforms to the ideal scenario and is commonly used in many applications. As the input energy has to be converted twice, the drawback of the two-stage approach is its low efficiency. To further optimize the conversion efficiency and reduce energy loss, the additional conversion loss induced by the two-stage structure can be reduced if the energy is transferred directly to the output load.

A system diagram of a parallel harvesting system is shown in Figure 8.24. The parallel structure aims to improve the conversion efficiency and retain the charging function. The parallel structure takes a primary path to convert energy directly to the load with the use of one-stage conversion to avoid additional conversion losses. The secondary path transfers the redundant energy to the storage device and performs the charging function when the energy source generates more energy than the load required. A DC/DC converter is placed after the battery to supply the primary path when the energy source is not fully adequate for the load.

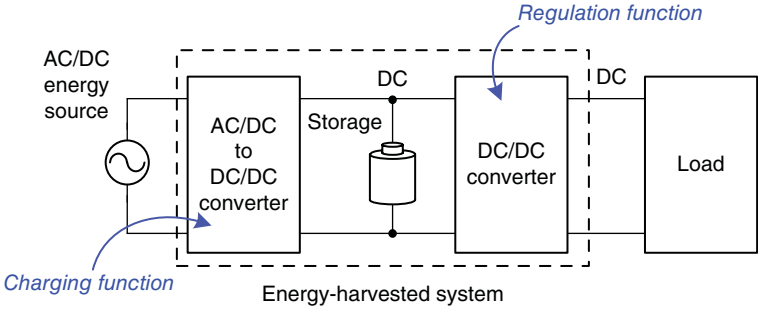

Figure 8.23 System diagram of a conventional serial harvesting system

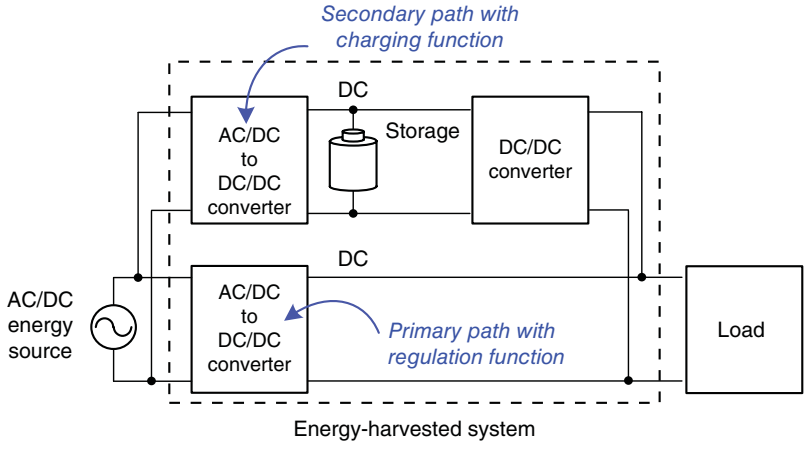

Figure 8.24 System diagram of a parallel harvesting system

However, the parallel structure introduces more design challenges than the conventional serial structure. First, the primary path AC/DC to DC/DC converter must have the ability to regulate the output voltage. Second, an energy distribution scheme is required to allocate the input energy to two paths accurately because the primary and secondary paths share the same energy source. Third, the extra circuits increase the overhead costs and the area.

Many harvesting circuits are similar to conventional power converters. Some of the main differences between an energy-harvesting circuit design and a conventional DC/DC or AC/DC converter design are summarized as follows:

1. The amount of energy from a source is limited. Thus, the loading condition of a system has to meet the characteristics of the energy-harvesting source.
2. An energy source is not a fixed voltage or a current source; it is a load or an environmental variant.
3. The input voltage may be very low or may vary across a wide range.
4. The operating voltage and the current have to be defined at the MPP.

In the following subsection the AC/DC to DC/DC converter, which can be used in Figures 8.23 and 8.24 with different functions and characteristics, will be introduced.

8.3.2 AC Source Energy-Harvesting Circuits

The design of an energy-harvesting circuit with an AC source has several objectives. The AC input must be rectified according to the DC value; otherwise, the energy harvested can hardly be used or stored. The magnitude of the AC source in a harvesting system varies correspondingly with environmental conditions. Thus, to protect the circuit from over-voltage damage, voltage limitations for some AC applications are required. The two-stage approach to AC source harvesting, which is depicted in Figure 8.23, is a mainstream approach and has been presented in previous publications. Depending on the input voltage and the current range,

AC/DC conversion needs to convert the input voltage to a proper voltage level for back-end usage. In the following subsections, the circuit description proceeds from the passive rectifier to the active rectifier. Afterward, some structures, which have combined the AC/DC to DC/DC converter and the DC/DC voltage regulator in recent years, are described. A presentation of the design concerns, with pros and cons, as regards each circuit follows shortly.

8.3.2.1 Full/Half Bridge Rectifier

The most straightforward and robust AC/DC converter is the conventional full bridge rectifier, which is shown in Figure 8.25. A passive full bridge rectifier needs no control and is very useful in harvesting applications. The harvesting system may run out of power and may have to be fully turned off to save energy. Passive components have no static power consumption, except when leakage occurs. Sometimes the input voltage under low-power conditions can hardly reach the turn-on voltage of the full bridge rectifier. Even if the input voltage is sufficient, the dropout voltages on the diodes seriously influence power efficiency when the input voltage is low. Schottky diodes with low forward voltage can improve the efficiency but suffer from reverse current leakage and reverse recovery leakage.

Charge Pump Rectifier

A voltage doubler charge pump, as shown in Figure 8.26, is similar to a full bridge rectifier [45,46]. As high-frequency-switching operation is power consuming and difficult to control

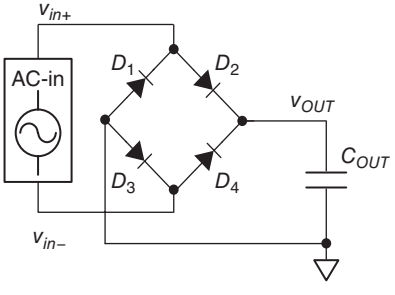

Figure 8.25 Full bridge rectifier

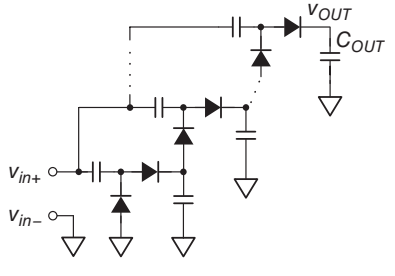

Figure 8.26 Voltage doubler charge pump

accurately, a fully passive structure has been used in high-frequency applications, such as RFID powering. The input voltage is automatically pumped to a higher level through cascading. Cascading is very useful for sources with relatively low output voltages. However, diode loss remains a serious issue for this circuit. If the diode forward voltage is V_D, then the output voltage is similar to that described in Eq. (8.28) for an N-stage charge pump:

$$V_{OUT} = N(V_{in} - 2V_D) + V_D \tag{8.28}$$

Each cascading stage suffers from dropout voltages. The higher the cascading stages, the larger the power losses that occur in the diodes. A considerable number of components results in a decrease in cost or area efficiency.

Active Rectifier

Active diode rectifiers control transistors as switches. The large diode forward voltage is replaced by the voltage drop of the transistor. Figure 8.27 shows a fully synchronous active rectifier. Two comparators are used to compare the voltage between the terminals, that is, V_{in+} and V_{in-}, and the output voltage V_{OUT}. When the terminal voltage is higher than V_{OUT}, the corresponding path is turned on to perform rectification. The minimum input voltage requirement constructed by the diode forward voltage can be released, and the diodes suffer from energy loss as well. However, the trade-off for the aforementioned advantages is the control circuit requirement. The control circuits must be powered first to turn on the active rectifier. Thus, the circuit cannot be fully turned off and cannot start up when the stored energy is exhausted. These trade-offs are not beneficial to high system sustainability.

MOSFET Rectifier with an Active Diode

Figure 8.28 shows a combination of passive and active rectifiers [47]. MOSFETs M_1 to M_4 act as a rectifier to select the proper turn-on path and translate AC input into DC output. The active diode is placed between the MOSFET rectifier and the output storage device to prevent a reverse current when V_{OUT} is higher than the terminal voltage of the AC input. This cascade structure has a forward voltage of one transistor threshold voltage (V_{th}). A standard diode

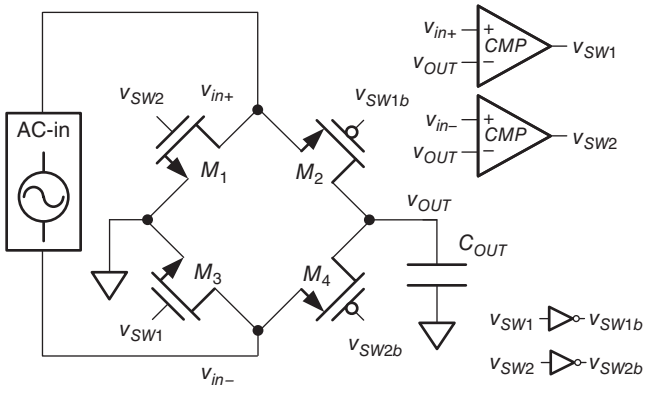

Figure 8.27 Fully synchronous active rectifier

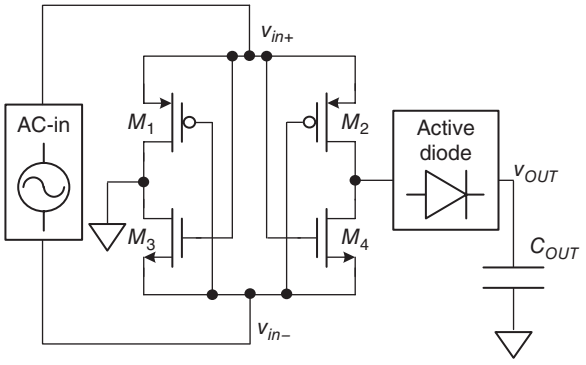

Figure 8.28 Passive MOS rectifier with active diode

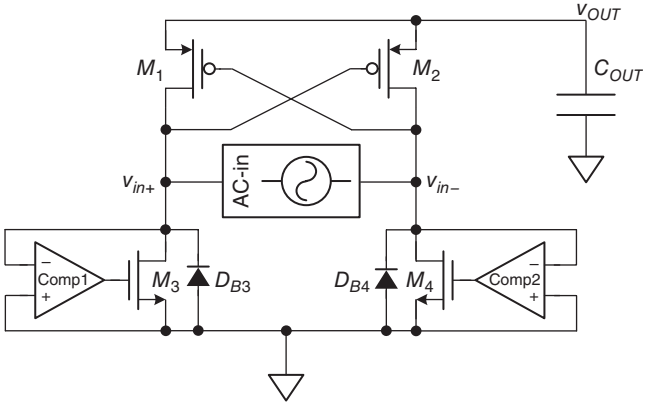

Figure 8.29 Diode-connected P-MOSFET with active N-MOSFET as rectifier

forward voltage is about the same as V_{th}. Compared with a conventional full bridge rectifier, a MOSFET rectifier with an active diode allows for one V_{th} of the forward voltage to be saved. Furthermore, the body diode of the MOSFET switch in the active diode can be used as a forward diode during start-up status. Thus, the combined structure can passively and automatically start up without any need for a power-on scheme even under zero energy condition.

Cross-Coupled P-MOSFET with Active N-MOSFET as Rectifier

Figure 8.29 shows another structure which uses diode-connected P-MOSFET and comparator-based N-MOSFET switches as the rectifier [48–50]. This structure has the same functions as those of the passive MOSFET rectifier with an active diode, but experiences less conduction loss for two reasons. First, the power path passes through two transistors, which is one less than the structure illustrated in Figure 8.28. Second, the N-MOSFET switch in Figure 8.29 has less average turn-on resistance than the N-MOSFET in the rectifier in Figure 8.28, because the gate of the N-MOSFET is controlled by the active circuit.

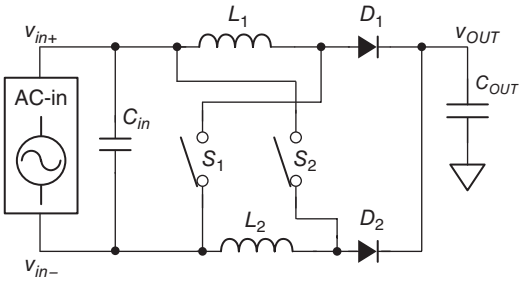

Figure 8.30 Dual-boost converter for AC/DC conversion

Dual-Boost AC/DC Converter

The aforementioned rectifier circuits only perform AC/DC conversion without any regulation capability. The output voltage level of the rectifier is determined by the input AC voltage. Thus, a rectifier that can simultaneously rectify and regulate the output voltage through the same circuit is a good option. Figure 8.30 shows the dual-boost converter for AC/DC conversion [51]. Two sets of boost converters operate alternately when the polarity of the AC input changes. The boost converter can be turned off when V_{OUT} exceeds the rated value. Thus, if the input energy is high enough to fully support the output loading, then the dual-boost structure has the ability to regulate V_{OUT} and can supply direct to the back-end system.

However, a trade-off occurs between zero energy start-up and regulation. The regulation function relies on the fully turned-off system to limit the energy being transferred. If the system is not powered first, the energy is prohibited from the harvesting source. The aforementioned passive rectifier as voltage doubler in Figure 8.26 could serve as a complement to help address this problem.

In terms of efficiency, the voltage doubler charge pump is not a good choice. However, given its fully passive and voltage-boost characteristics, the voltage doubler charge pump is a good option for a start-up circuit. If the harvesting system starts from zero energy, the voltage doubler charge pump can provide a voltage that will drive the control circuit in the start-up state. Afterward, a more efficient converter can be used instead of the charge pump. Many harvesting systems need this kind of "handover" scheme to start up the system from zero energy and improve the efficiency when normal operation is available. The handover structure can extend the sustainability of the system to a theoretically unlimited range. The system can operate again as long as adequate energy comes from the harvester.

Single-Inductor Dual-Boost Converter

Figure 8.31 is a modified type of the dual-boost structure in Figure 8.30 [52]. By arranging the switches, that is, S_1 and S_2, and the diodes, both boost converters share an inductor. This approach reduces bulky external components while maintaining the same functionality of the dual-boost structure.

Single-Inductor Buck/Boost Converter

Different energy sources have different output voltages. For general-purpose power conversion, Figure 8.32 shows a single-inductor buck/boost converter [53]. The buck/boost structure

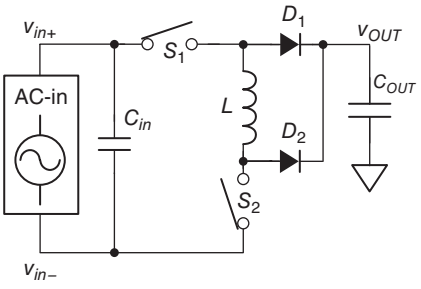

Figure 8.31 Single-inductor dual-boost converter

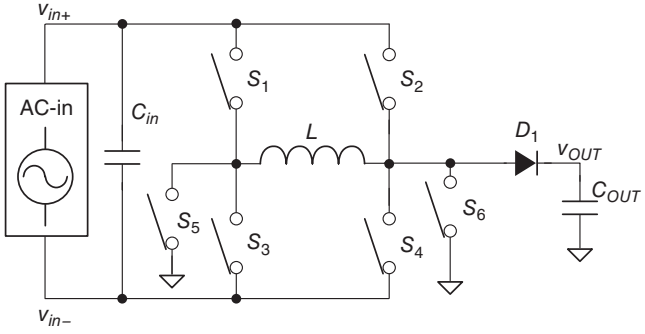

Figure 8.32 Single-inductor buck/boost converter

has the ability to up-convert or down-convert the input voltage, which provides more flexibility to the selection of energy-harvesting sources. The input voltage level is not limited by the converter structure. The diodes in Figures 8.30–8.32 can be replaced by active diodes to further enhance conversion efficiency.

Energy sources may not have the capability to store electric charge. In switch-based harvesting circuits, sudden current extraction from the inductor causes a considerable voltage drop in the energy-harvesting source. Sometimes the voltage drop is too large, so that it could cause reverse leakage or influence the normal operation of the converters. Thus, an input capacitor C_{In} is necessary for inductor-based converters. Energy from the energy source can be stored in C_{In} as a buffer to maintain a relatively stable voltage.

Summary of AC-Source Energy-Harvesting Circuits

Figure 8.33 shows a diagram summarizing and comparing the characteristics and functions of the structures discussed in this subsection. The rectifiers and converters are listed in the order of high-power loss to low-power loss and divided by different function requirements. Figure 8.33 provides simple instructions to help filter the possible structures and proceed with the harvesting circuit design.

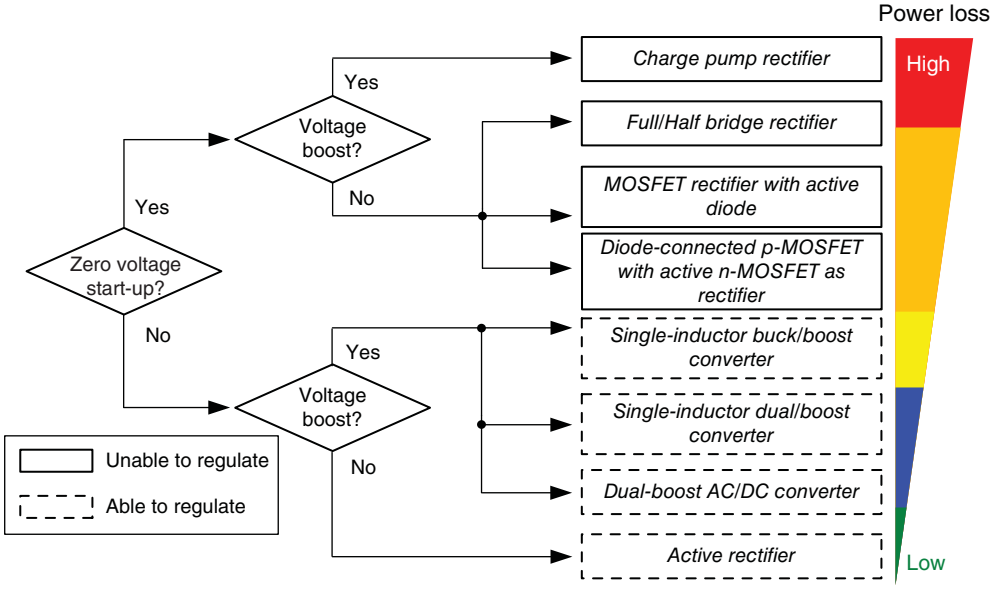

Figure 8.33 Function selection and characteristics of different AC/DC structures

8.3.3 DC-Source Energy-Harvesting Circuits

In energy harvesting, the number of AC sources is larger than that of DC sources. The most widely discussed DC harvesting sources include TEGs and solar cells. The goal of a DC harvesting circuit is to convert the input voltage to a proper and regulated voltage level for battery charging or system supply. DC-source harvesting circuits are simpler than AC-source harvesting circuits. The former are similar to conventional DC/DC converters. DC/DC harvesting circuits can also be used as DC/DC converters that perform voltage regulation, as in Figures 8.23 and 8.24. Some concerns about converters in energy-harvesting applications will be discussed in Section 8.4.

8.3.3.1 Low-Dropout Regulator

The most attractive features of an LDO regulator are low noise, compact size, and fast transient response. Figure 8.34 shows the circuit of an LDO regulator. From Figure 8.34, an LDO regulator is clearly quite simple if no special specification is required. With fewer external components, the LDO regulator is efficient in terms of area and cost. Without switching in the power transistors and the high loop gain, LDO demonstrates great noise immunity, which is especially important for implanted biomedical signal-sensing applications. For example, sensing systems using small physiological signals, such as EEG, are noise sensitive and volume limited. For such applications, LDO is a good option as a power management unit.

LDO has the following drawbacks: (i) low efficiency and (ii) performance limited to step-down conversion. The low supply voltage generated by some harvesting sources also limits the use of LDO, especially when a battery-charging function is required. The efficiency of LDO

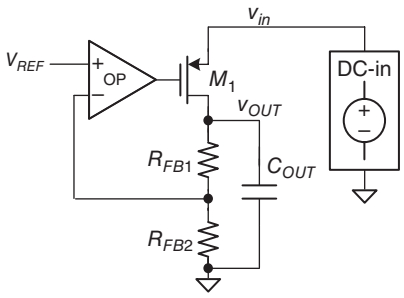

Figure 8.34 LDO regulator

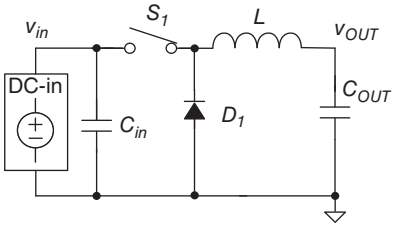

Figure 8.35 Buck converter

depends on the difference in input and output voltages. When the input voltage is high and the output is low, most of the energy is wasted on the power transistor because of the large dropout voltage. However, the low quiescent power of DC/DC voltage regulators makes linear regulators a good choice for low-power systems.

Buck Converter

Similar to LDOs, buck converters can provide step-down conversion. Figure 8.35 shows the power stage of a standard buck converter [54]. The characteristics of a switching converter allow for high efficiency but result in switching noise.

Boost Converter

Energy-harvesting sources, such as TEGs, have a very low DC voltage. A single solar cell provides a higher voltage of up to 1 V (open circuit). However, such a voltage is still not sufficient to charge batteries. Boost converters have been a straightforward solution, commonly used in many previous works [54]. Figure 8.36 shows a schematic of a boost converter. Boost converters have the advantage of high efficiency and output voltage regulation capability. Boost converters can function as a battery charger or even directly supply the load system.

Buck/Boost Converter

As shown in Figure 8.32, a buck/boost converter provides more flexibility to both input and output voltage ranges [54]. Figure 8.37 shows a schematic of a non-inverting buck/boost

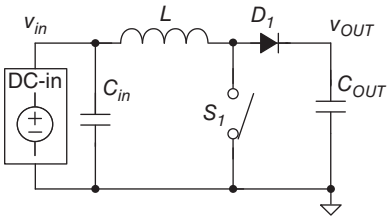

Figure 8.36 Boost converter

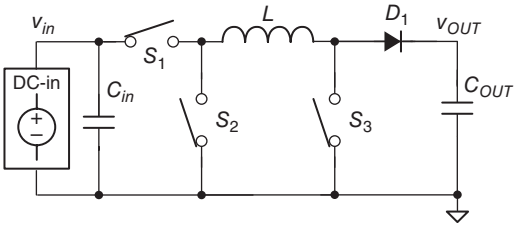

Figure 8.37 Buck/boost converter

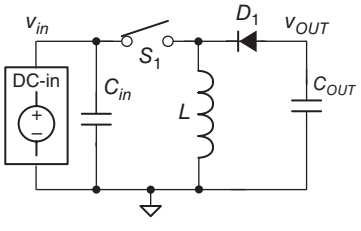

Figure 8.38 Inverting buck/boost converter

converter. The drawbacks of this converter are efficiency degradation caused by the extra pass transistors and the driving losses induced by extra switches.

Inverting Buck/Boost Converter

Figure 8.38 shows a schematic of an inverting buck/boost converter [54]. Inverting buck/boost converters have fewer switches, which results in higher efficiency. As the output voltage is inverted, the controller and the gate driving circuit for switches have to be designed especially. Such specification results in an increase in production costs.

Charge Pump

Aside from inductor-based converters, capacitor-based converters, such as charge pumps, are also widely used in energy-harvesting circuits. Figure 8.39 shows a 2 × boost charge pump circuit. If the circuit is cascaded, a high-voltage boost ratio can be achieved [55,56]. Charge pumps can also perform voltage regulation through a closed-loop control.

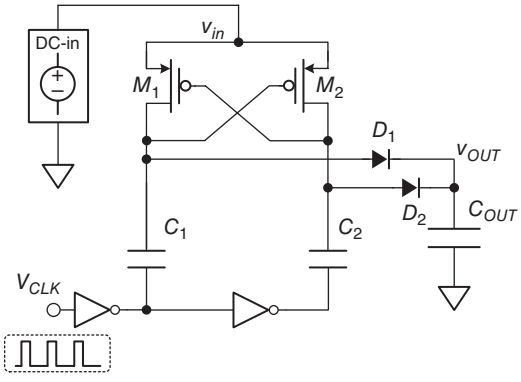

Figure 8.39 Charge pump step-up converter

Summary of DC-Source Energy-Harvesting Circuits

DC/DC harvesting circuits have the same design goals as those of conventional DC/DC converters. However, quiescent power is a more pressing issue for harvesting circuits than for conventional DC/DC converters. DC/DC converters may need sub-circuits to provide a reference voltage or a bias current to provide regular support to the DC/DC converter. These sub-circuits, such as bandgap voltage reference, comparators, or amplifiers, consume considerable power. The power loss may reach up to hundreds of microwatts. For DC/DC converters, which convert a large output power or require a fast transient response, the large power consumption caused by the controller is necessary. By contrast, the power consumption of low-input power applications, such as harvesting functions, might not be affordable or may even exceed the possible derived input power. Thus, one of the challenges in designing DC/DC harvesting circuits is how to design an ultra-low-power control circuit and operation scheme.

8.4 Maximum Power Point Tracking

8.4.1 Basic Concept of Maximum Power Point Tracking

Harvesting sources, such as PV cells, TEGs, vibration, or magnetic coils, have their own electrical and mechanical properties. The output voltage, current, and power of each source are influenced by the loading effect. Under a steady environmental condition, each source has a corresponding output voltage and current value to generate maximum output power. The point at which the maximum output power is generated is selected as the MPP, and the equivalent load at that point should be defined and tracked through MPPT control [1, 23, 30].

Using the equivalent model of solar cells in Figure 8.16 as reference, the current I_L generated by the solar cells is assumed constant in steady irradiation conditions. If the load on the output voltage V_{PV} is light, V_{PV} rises to a higher voltage, which induces current leakage on the parasitic diode D_S and the resistor R_{SH}. Conversely, if the load is heavy, V_{PV} drops to a low level, and most of the power is wasted on the series resistor R_S. Thus, identifying the MPP is important to extract the maximum possible power under the same environmental conditions. Many harvesting systems utilize MPPT circuits to enhance efficiency and derive maximum output power

[1,21–23,25,35]. However, the following should be noted regarding a harvesting system with the MPPT function:

1. The characteristic of the energy sources must be known before applying the MPPT method.
2. The power consumption of the MPPT circuit is critical for numerous low-power applications.
3. MPPT control fixes the input source at its maximum output energy.
4. A storage device is necessary for harvesting systems that adopt the MPPT function.
5. Continuous tracking is necessary to overcome environmental condition variations. MPP varies under different environmental conditions. The harvesting circuits should control the power-delivery condition to ensure that the energy-harvesting system operates at its MPP.

The MPPT scheme is a method of tracking input power. If a harvesting system supplies voltage directly to the load system, the MPPT function hinders the harvesting system from regulating the output voltage at the same time unless the input power is always the same as the load requirement, which is unlikely. Thus, some general ideas and methods for implementing the MPPT control are presented in the following subsections.

8.4.2 *Impedance Matching*

Many harvesting sources have complex behaviors or internal equivalent circuit models. Prior studies, for example [23,25,52,57], have presented numerous optimized designs for different sources and characteristics; these circuits can only be used on the specific sources they are designed for. The impedance-matching method is the most popular and important approach for a general-purpose MPPT. Figure 8.40 shows the Thevenin equivalent circuit of an energy-harvesting source modeled as an ideal voltage source, V_{EQ}, with series resistance R_S. Generally, all sources can be modeled as in Figure 8.40, with different Thevenin equivalent impedance even if the impedance is not pure resistance and includes inductance and capacitance. However, the idea of matching the load impedance with the inner impedance is still valid and provides tracking instructions when MPPT is desired.

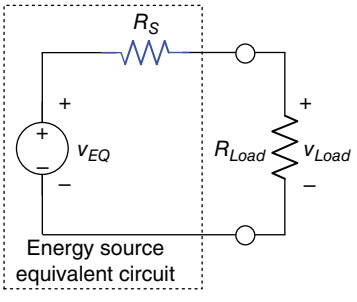

Figure 8.40 Thevenin equivalent circuit of energy source

The power P_{Load} on the output loading R_{Load} is shown as:

$$P_{Load} = V_{Load}^2 R_{Load} = \left(\frac{V_{EQ}}{R_S + R_{Load}}\right)^2 R_{Load} \tag{8.29}$$

Impedance-matching theory implies that the system achieves maximum power transfer when the loading impedance is equivalent to the inner impedance. The maximum output power transferred to the load, $P_{Load,max}$, is expressed as in Eq. (8.30). Matching efficiency is defined as the ratio of the power in the load to the maximum output power, as shown in Eq. (8.31):

$$P_{Load,max} = \frac{V_{EQ}^2}{4R_{Load}} \tag{8.30}$$

$$\frac{P_{Load}}{P_{Load,max}} = \frac{4}{2 + \frac{R_{Load}}{R_S} + \frac{R_S}{R_{Load}}} \tag{8.31}$$

Figure 8.41 shows matching efficiencies at different impedance errors. An impedance error represents the mismatch percentage compared with the inner impedance of the harvesting source. When the load impedance is perfectly matched with the inner impedance, the error percentage is zero and the matching efficiency is unity. If 90% matching efficiency is desired, the endurable load impedance error ranges from −48 to +93%. This large endurable range indicates that even if a large error percentage occurs, the output power remains very close to the MPP.

8.4.3 Resistor Emulation

An equivalent resistance of the converter can be obtained if the ratio of the input voltage to the average input current is considered, regardless of whether switching or linear power converters are adopted. This scheme is called resistance emulation [23,25,30,58]. The equivalent resistance can be derived by calculating the average input current during the operation of a converter.

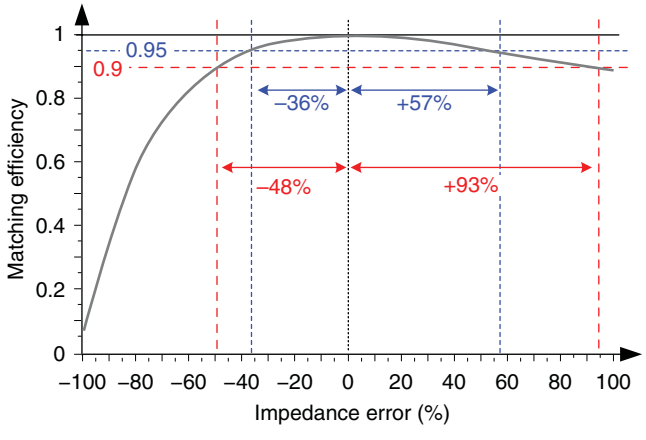

Figure 8.41 Matching efficiency versus impedance error

For example, if the buck/boost converter in Figure 8.37 with constant switching frequency PWM control is operated in DCM, the charging and discharging phases of the buck/boost converter are as shown in Figure 8.42. The behavior of the inductor current when the input voltage changes is shown in Figure 8.43.

The buck/boost converter only connects to the input voltage source in the charging phase, where I_{Peak} is the peak current in the charging phase. The average input current of the converter, $I_{in,avg}$, is defined by Eq. (8.32), where D is the duty cycle, T is the time of a switching period, and L is the inductor used in the converter:

$$I_{in,avg} = \frac{I_{Peak} \cdot D}{2T} = \frac{V_{in} T \cdot D^2}{2L} \tag{8.32}$$

The input voltage V_{in} is divided by $I_{in,avg}$ to derive the equivalent resistance R_{eq} as shown in Eq. (8.33), which is related to D and T:

$$R_{eq} = \frac{V_{in}}{I_{in,avg}} = \frac{2L}{T \cdot D^2} \tag{8.33}$$

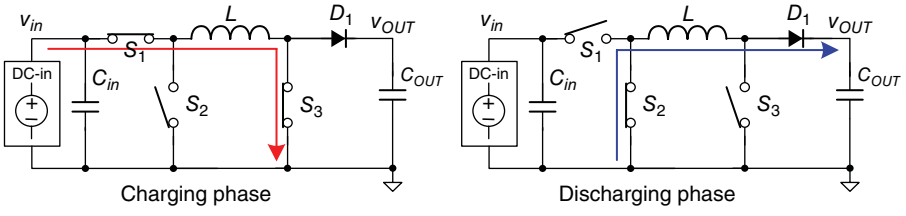

Figure 8.42 The buck/boost converter operation

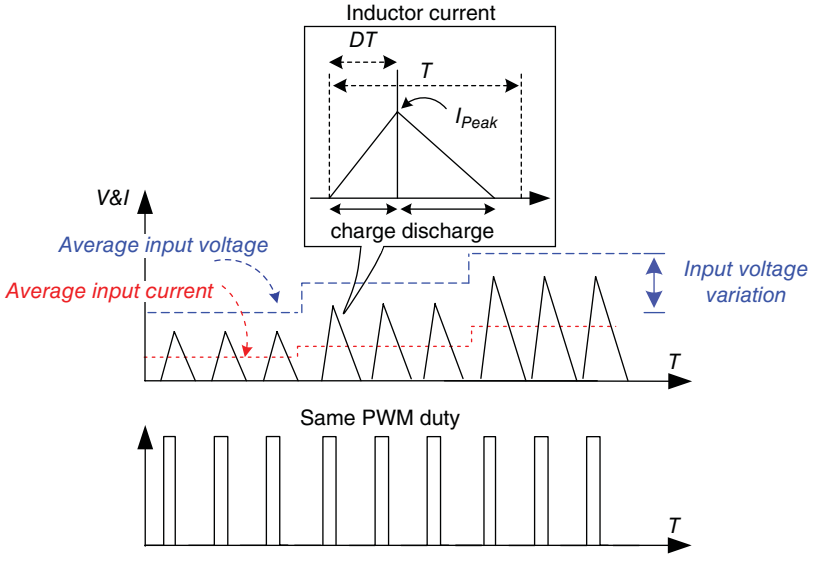

Figure 8.43 Inductor current under DCM operation

The duty or switching frequency can be used to adjust R_{eq} through PWM or PFM control. Thus, the converters can be considered a tunable resistance to match the inner impedance and obtain maximum output power.

Several considerations should be noted regarding the resistance emulation method. Converter parameters should be selected appropriately. R_{eq} should fit the inner impedance of the harvesting source. The coverage range of R_{eq} should be designed according to the target source. If a switching converter is used as the emulated resistor, a low switching frequency will induce a large switching current ripple. If the driving capability of the energy source is insufficient to sink the current, then the terminal of the source will drop significantly. The large voltage variation in some energy sources, such as solar cells, which have complex equivalent internal models, influences the output power condition. Even if the equivalent resistance is the ratio of the average input voltage to the current, the large voltage variation may result in additional power loss or power conditions deviating from the MPP.

8.4.4 MPPT Method

Different harvesting sources require different tracking methods to achieve the MPP. The resistor emulation introduced in Section 8.4.3 enables MPPT controllers to control the energy sources to achieve energy at their respective MPPs. In resistor emulation, the MPPT controller adjusts the resistor emulation converter control factors, such as the duty or the frequency. The adjustment changes the emulated loading to match the characteristics of the harvesting source. The MPPT method is the procedure used to perform adjustment.

8.4.4.1 Mountain-Climbing (Perturb and Observe) Method

The commonly used MPPT method for harvesting sources with complex models and behaviors is the mountain-climbing method, which is also called the perturb and observe (P&O) method [23,30]. This method is applied to solar cells because of the complex relationship between their operating environment and the maximum power. The MPPT operation on a solar cell is illustrated in Figure 8.44. The output power is measured after each adjustment. If the power

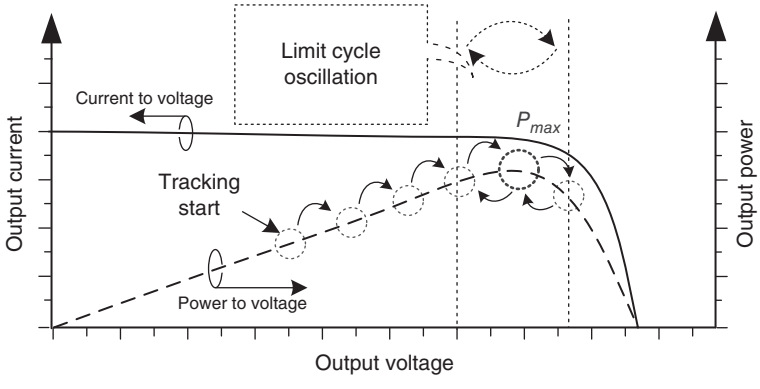

Figure 8.44 MPPT of solar cells

increases, then further adjustment in the same direction is performed until the power no longer increases. This method is so named because it is similar to mountain climbing and it depends on the rise of the power versus voltage curve below the MPP. Once the adjustment exceeds the MPP, the output power will fall below the MPP. The adjustment turns to the opposite direction and traces back to the MPP. The tracking operation goes back and forth around the MPP. To track the output power continuously, adjustment should be performed regularly to deal with environmental variations. Thus, if the environmental condition is stable, the adjustment is in a limiting cycle oscillation.

Figure 8.45 shows a flowchart of MPPT. In some applications, if the MPP curve has more than one peak value, the mountain-climbing method may suffer from a local optimization problem. This indicates that the tracked MPP is not the global optimization in the MPP curve but the local optimization. The tracking flow cannot detect whether it is located at the global optimization or at the local optimization. P&O is the most commonly used MPPT method because of its ease of implementation and flexibility with different applications.

To ensure the appropriateness of adjustments, the mountain-climbing method should constantly sample and monitor the output power condition. Sampling and monitoring are the most challenging parts of this method. A set of data converters is conventionally used to sample the output current and voltage in an electricity-generating solar cell array. Such data conversion and calculation is also applied to solar energy-harvesting applications, as shown in Figure 8.46. Information on the sampled current and power is calculated by the processor and then stored in the memory to control the tracking strategy. This method is very straightforward and has the advantage of high accuracy. The same method can also be applied to the output part. In monitoring the output current and voltage, the output power also represents the status of the input source, as shown in Figure 8.47 [43].

However, continuous data conversion and digital signal processing with storage are power consuming. For low-power energy-harvesting applications, the considerable power consumed by the tracking method significantly influences the derived output power. Some low-input power applications use the characteristics of the switching power converter to monitor the power status without complex data conversion and calculation. Figure 8.48 shows the peak

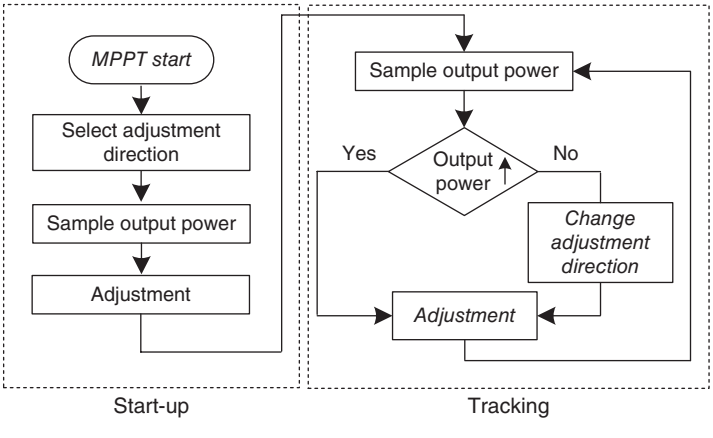

Figure 8.45 MPPT flowchart

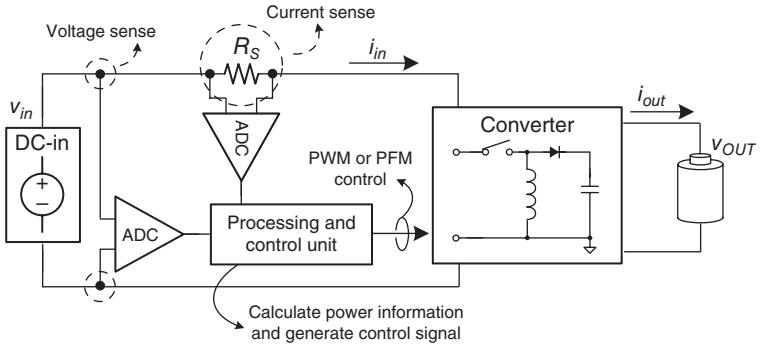

Figure 8.46 Input power-monitoring scheme

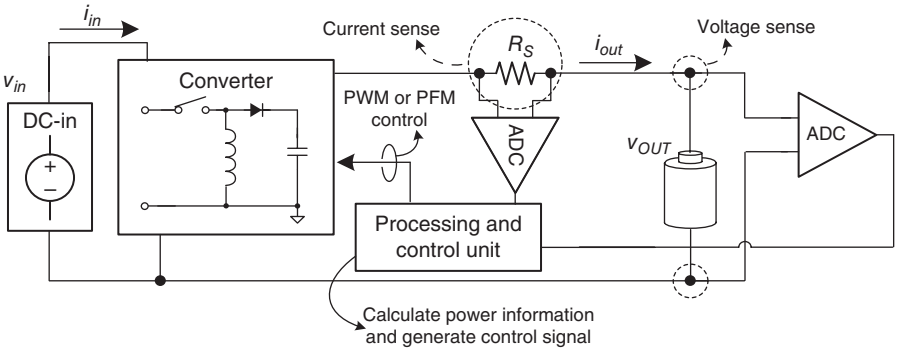

Figure 8.47 Output power-monitoring scheme

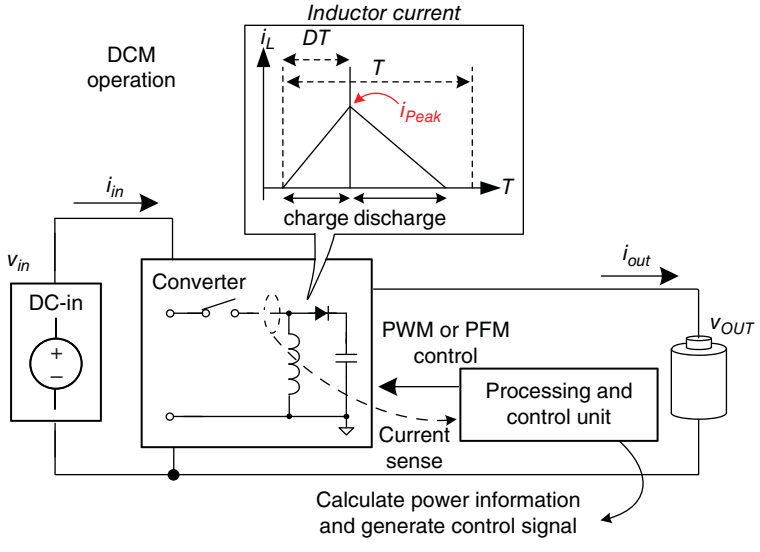

Figure 8.48 Peak inductor current output power-monitoring scheme

inductor current-monitoring method [53,59]. If the power converter operates in the DCM, the energy stored in the inductor of each cycle will be delivered completely to the output, which means that the output power is proportional to the peak current. By using a current-sensing circuit in the power converter, the peak current, I_{Peak}, can be used as an index to verify the power condition. The aforementioned power-sensing methods can only be used under certain converter structures and operating modes.

8.4.4.2 Open-Circuit Test Method

For energy sources with fixed built-in resistances, the MPP is proportional to the open-circuit voltage. The most commonly discussed energy source that applies the open-circuit test method is a TEG [25,27]. Figure 8.49 shows the current I_{TEG} and the power P_{TEG} over the voltage of the TEG. The same idea of impedance matching is applied in this method, that is, maximum power exists when the inner resistance is the same as the load resistance. According to voltage divider theory, the MPPT voltage is approximately half the open-circuit voltage.

Figure 8.50 shows a block diagram of a harvesting system that applies the open-circuit test method. As the name of the method implies, power monitoring and sampling are achieved by opening the circuit from the harvesting source during the sampling period. A comparison of the sampled voltage with the closed-circuit voltage is achieved under operation.

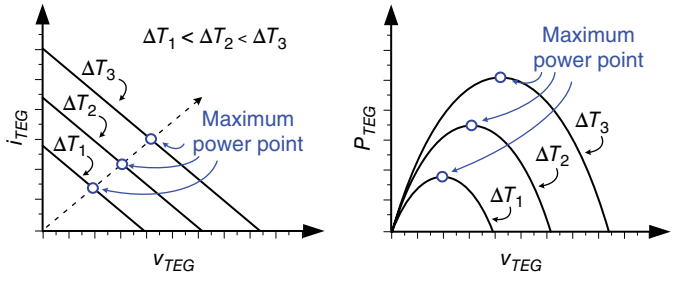

Figure 8.49 The current I_{TEG} and the power P_{TEG} over the voltage of the TEG

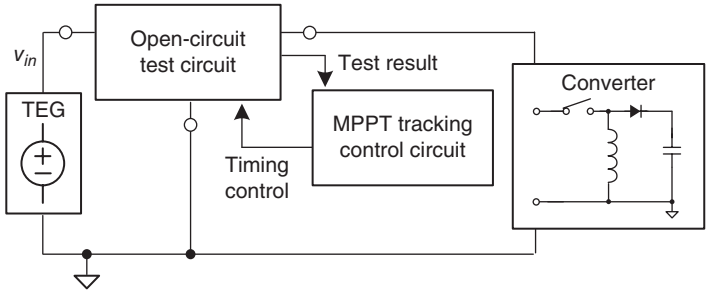

Figure 8.50 Open-circuit test method and system diagram

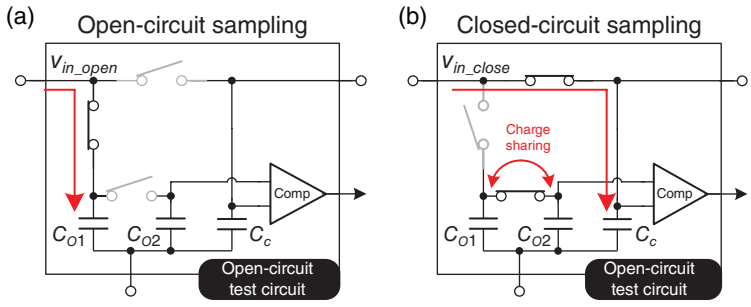

Figure 8.51 Circuit implementation of (a) open-circuit sampling and (b) closed-circuit sampling

Owing to the limited driving capability of the energy source and the operating speed of the converter in both open- and closed-circuit sampling, the output voltage of the energy source requires transient time to achieve the steady-state voltage. The recovery time is source dependent and should be considered in the sampling timing control. The implementation of the open-circuit test method is shown in Figure 8.51. The circuit operations during open-circuit sampling and closed-circuit sampling are shown in Figure 8.51(a) and (b), respectively. C_{O1} and C_{O2} have the same capacitance values and perform charge sharing to derive half of the open-circuit voltage, V_{in_open}. The closed-circuit voltage, V_{in_close}, is compared with the divided V_{in_open} to define the power condition. The converter adjusts the emulated resistance according to the comparison result. If the divided V_{in_open} is higher than V_{in_close}, then the emulated resistance is extremely high. By contrast, if V_{in_open} is lower than V_{in_close}, then the emulated resistance is extremely low. The open-circuit test method is also used in solar cell MPPT, but it adopts a different divider ratio of 0.7. The MPP of a solar cell is often near 0.7 of its open-circuit voltage. Thus, compared with the slow mountain-climbing procedure, the open-circuit test can approach the MPP relatively quickly.

8.4.4.3 Iterative-Based MPPT

The mountain-climbing method saves and compares the power status after each sampling and adjustment. The iterative-based MPPT method shifts the comparison from the previous sampled power status to a dynamic target power through the following procedure. First, the target power traces the present sampled power status. The target power level is then promoted and the converted power is adjusted to approach the target. The procedure is repeated, and the power target and the sampled power status iteratively track each other to reach the MPP [53].

In this method, the DCM in Figure 8.48 is taken as a converter example and the PWM duty is utilized as the control factor. Figure 8.52 shows the tracking operation. A target power represented by a voltage signal, V_{Target}, is compared with the peak of the current sense signal V_{CS}. At the beginning, V_{Target} is set higher than V_{CS}. The time-out period, T_O, is designed as the settling time for the converter and the energy-harvesting source. If V_{Target} and V_{CS} encounter each other within the time-out period, V_{Target} will be set to a lower level. Through several comparisons, V_{Target} will approach V_{CS}. Meanwhile, V_{Target} represents the recent power status. Afterward, V_{Target} is set to a slightly higher level as a new target for V_{CS}. The MPPT controller adjusts

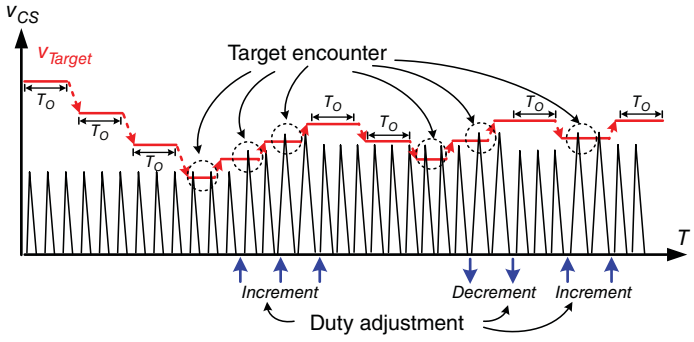

Figure 8.52 Target power and sampled power status iteratively track each other

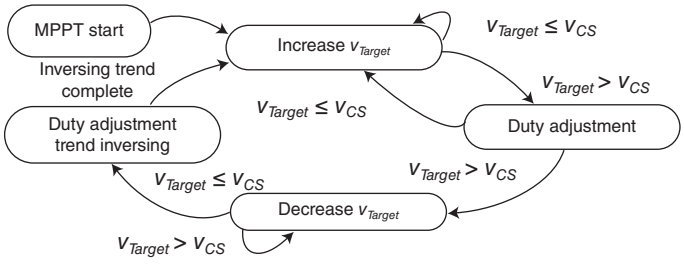

Figure 8.53 FSM of iterative-based tracking

the PWM duty and checks the V_{CS} variation. The adjustments may cause the output power to either rise or fall. V_{CS} reaching V_{Target} before the time-out period indicates that the output power is rising and the duty-adjusting trend is correct. V_{Target} shifts to a higher level and is set to a new target. The adjusting trend continues in the same direction. However, if V_{CS} does not reach V_{Target}, an incorrect adjusting trend occurs. After the time-out period, the MPPT controller lowers the V_{Target} to find the V_{CS} and to change the adjusting trend. In conclusion, V_{Target} is always set to a slightly higher target compared with the recent input power condition. Figure 8.53 shows the FSM of the iterative-based MPPT control.

References

[1] Priya, S. and Inman, D.J. (2009) *Energy Harvesting Technologies*. Springer-Verlag, New York.
[2] Yang, Y., Lambert, F., and Divan, D. (2007) A survey on technologies for implementing sensor networks for power delivery systems. *Proceedings of the IEEE Power Engineering Society General Meeting*, June, pp. 1–8.
[3] Roundy, S.J. (2003) Energy scavenging for wireless sensor nodes with a focus on vibration to electricity conversion. PhD thesis, University of California, Berkeley, CA.
[4] Paradiso, A. (2008) Energy Scavenging for Mobile and Wireless Electronics. Massachusetts Institute of Technology Media Laboratory Thad Starner, Georgia Institute of Technology, GVU Center.
[5] Mateu, L. and Moll, F. (2005) Review of energy harvesting techniques and applications for microelectronics. *Proceedings of SPIE*, **5837**, 359–373.
[6] Meindl, J. (1995) Low power microelectronics: Retrospect and prospect. *Proceedings of the IEEE*, **83**, 619–635.

[7] Rabaey, J., Ammer, J., Karalar, T., *et al*. (2002) Picoradios for wireless sensor networks: The next challenge in ultralow-power design. *IEEE International Solid-State Circuits Conference (ISSCC)*, *Digest of Technical Papers*, San Francisco, CA, February 3–7, pp. 200–201.
[8] Calhoun, B., Daly, D., Verma, N., *et al*. (2005) Design considerations for ultra-low energy wireless microsensor nodes. *IEEE Transactions on Computers*, **54**(6), 727–740.
[9] Chapman, P. and Raju, M. (2008) Designing power systems to meet energy harvesting needs. *TechOnline India*, **8**(42).
[10] Paulo, J. and Gaspar, P.D. (2010) Review and future trend of energy harvesting methods for portable medical devices. *Proceedings of the World Congress on Engineering (WCE)*, San Francisco, CA, October, Vol. **2**.
[11] Huang, T.-C., Hsieh, C.-Y., Yang, Y.-Y., *et al*. (2012) A battery-free 217 nW static control power buck converter for wireless RF energy harvesting with α-calibrated dynamic on/off time and adaptive phase lead control. *IEEE Journal of Solid-State Circuits*, **47**, 852–862.
[12] Zhang, X.Y., Jiang, H.J., Zhang, L.W., *et al*. (2010) An energy-efficient ASIC for wireless body sensor networks in medical applications. *IEEE Transactions on Biomedical Circuits and Systems*, **3**(1), 11–18.
[13] Moore, G.E. (1998) Cramming more components onto integrated circuits. *Proceedings of the IEEE*, **86**, 82–85.
[14] ZigBee Alliance (2006) ZigBee Specifications, Version 1.0 r13, December. http://www.zigbee.org/(accessed November 13, 2015).
[15] Institute of Electrical and Electronics Engineers, Inc. IEEE Std. 802.15.4- 2003 (2003) IEEE Standard for Information Technology—Telecommunications and Information Exchange between Systems—Local and Metropolitan Area Networks—Specific Requirements—Part 15.4: Wireless Medium Access Control (MAC) and Physical Layer (PHY) Specifications for Low Rate Wireless Personal Area Networks (WPANs). Institute of Electrical and Electronics Engineers, Inc., New York.
[16] Banerjee, K., Souri, S.J., Kapur, P., and Saraswat, K.C. (2001) 3-D ICs: A novel chip design for improving deep-submicrometer interconnect performance and systems-on-chip integration. *Proceedings of the IEEE*, **89**(5), 602–633.
[17] Pereyma, M. (2007) *Overview of the modern state of the vibration energy harvesting devices*. Proceedings of the International Conference on Perspective Technologies and Methods in MEMS Design, May, pp. 107–112.
[18] Cheng, S., Wang, N., and Arnold, D.P. (2007) Modeling of magnetic vibrational energy harvesters using equivalent circuit representations. *Journal of Micromechanics and Microengineering*, **17**, 2329–2335.
[19] Anderson, M.J., Cho, J. H., Richards, C.D., *et al*. (2005) A comparison of piezoelectric and electrostatic electromechanical coupling for ultrasonic transduction and power generation. *Proceedings of the IEEE Ultrasonics Symposium*, pp. 950–955.
[20] Flynn, A.M. and Sanders, S.R. (2002) Fundamental limits on energy transfer and circuit considerations for piezoelectric transformers. *IEEE Transactions on Power Electronics*, **17**, 8–14.
[21] Koutroulis, E. and Kalaitzakis, K. (2006) Design of a maximum power tracking system for wind-energy-conversion applications. *IEEE Transactions on Industrial Electronics*, **53**, 486–494.
[22] Tan, Y.-K. and Panda, S.K. (2011) Self-autonomous wireless sensor nodes with wind energy harvesting for remote sensing of wind-driven wildfire spread. *IEEE Transactions on Power Electronics*, **26**(4), 1367–1377.
[23] Tan, Y.-K. and Panda, S.K. (2011) Optimized wind energy harvesting system using resistance emulator and active rectifier for wireless sensor nodes. *IEEE Transactions on Power Electronics*, **26**(1), 38–50.
[24] Roundy, S., Steingart, D., Frechette, L., *et al*. (2004) Power sources for wireless sensor networks. Presented at the *Proceedings of 1st European Workshop on Wireless Sensor Networks (EWSN)*, Berlin, Germany.
[25] Ramadass, Y.K. and Chandrakasan, A.P. (2011) A battery-less thermoelectric energy harvesting interface circuit with 35 mV startup voltage. *IEEE Journal of Solid-State Circuits*, **46**(1), 333–341.
[26] Carlson, E.J., Strunz, K., and Otis, B.P. (2009) A 20 mV input boost converter with efficient digital control for thermoelectric energy harvesting. *IEEE Journal of Solid-State Circuits*, **45**(4), 741–750.
[27] Tellurex (N.D.) Thermoelectric Generators. http://www.tellurex.com/(accessed November 14, 2015).
[28] Kishi, M., Nemoto, H., Hamao, T., *et al*. (1999) Micro thermoelectric modules and their application to wristwatches as an energy source. *Proceedings of the International Conference on Thermoelectrics*, pp. 301–307.
[29] Lineykin, S. and Ben-Yaakov, S. (2007) Modeling and analysis of thermoelectric modules. *IEEE Transactions on Industry Application*, **43**(2), 505–512.
[30] Bandyopadhyay, S. and Chandrakasan, A.P. (2012) Platform architecture for solar, thermal, and vibration energy combining with MPPT and single inductor. *IEEE Journal of Solid-State Circuits*, **47**(9), 2199–2215.
[31] Schoeman, J.J. and van Wyk, J.D. (1982) A simplified maximal power controller for terrestrial photovoltaic panel arrays. *IEEE Power Electronics Specialists Conference*, pp. 361–367.

[32] Sullivan, C.R. and Powers, M.J. (1993) A high-efficiency maximum power point tracker for photovoltaic arrays in a solar-powered race vehicle. *IEEE Power Electronics Specialists Conference*, pp. 574–580.
[33] Esram, T. and Chapman, P.L. (2007) Comparison of photovoltaic array maximum power point tracking techniques. *IEEE Transactions on Energy Conversion*, **22**(2), 439–449.
[34] Ziegler, S., Woodward, R.C., Iu, H.H.-C., and Borle, L.J. (2009) Current sensing techniques: A review. *IEEE Sensors Journal*, **9**(4), 354–376.
[35] Paing, T., Falkenstein, E., Zane, R., and Popovic, Z. (2009) Custom IC for ultra-low power RF energy harvesting. IEEE Applied Power Electronics Conference and Exposition (APEC 2009), pp. 1239–1245.
[36] Smith, A.A. (1998) *Radio Frequency Principles and Applications: The Generation*, *Propagation*, *and Reception of Signals and Noise*. IEEE Press, New York.
[37] Ungan, T. and Reindl, L. (2008) Harvesting low ambient RF-sources for autonomous measurement systems. *Proceedings of the IEEE International Instrumentation and Measurement Technology Conference (IMTC)*, pp. 62–65.
[38] Nintanavongsa, P., Muncuk, U., Lewis, D.R., and Chowdhury, K.R. (2012) Design optimization and implementation for RF energy harvesting circuits. *IEEE Journal on Emerging and Selected Topics in Circuits and Systems*, **2**(1), 24–33.
[39] Williams, C.B. and Yates, R.B. (1996) Analysis of a micro-electric generator for microsystems. *Sensors and Actuators*, **52**(1–3), 8–11.
[40] Maurath, D., Becker, P.F., Spreemann, D., and Manoli, Y. (2012) Efficient energy harvesting with electromagnetic energy transducers using active low-voltage rectification and maximum power point tracking. *IEEE Journal of Solid-State Circuits*, **47**(6), 1369–1380.
[41] Arroyo, E. and Badel, A. (2011) Electromagnetic vibration energy harvesting device optimization by synchronous energy extraction. *Sensors and Actuators A: Physical*, **171**(2), 266–273.
[42] Roundy, S., Wright, P.K., and Rabaey, J. (2002) Micro-electrostatic vibration-to-electricity converters. *Proceedings of the ASME 2002 International Mechanical Engineering Congress and Exposition*, pp. 487–496.
[43] Huang, T.-C., Lee, Y.-H., Du, M.-J., *et al*. (2012) A photovoltaic system with analog maximum power point tracking and grid-synchronous control. *Proceedings of the IEEE 15th International Power Electronics and Motion Control Conference (EPE/PEMC)*, September, pp. LS1d.3-1–LS1d.3-6.
[44] Kurs, A., Karalis, A., Moffatt, R., *et al*. (2007) Wireless power transfer via strongly coupled magnetic resonances. *Science Express*, **317**(5834), 83–86.
[45] Nakamoto, H., Yamazaki, D., Yamamotot, T., *et al*. (2006) A passive UHF RFID tag LSI with 36.5% efficiency CMOS-only rectifier and current-mode demodulator in 0.35 μm FeRAM technology. *IEEE International Solid-State Circuits Conference (ISSCC)*, *Digest of Technical Papers*, San Francisco, CA, February 3–7, pp. 310–311.
[46] Yi, J., Ki, W.-H., Mok, P.K.T., and Tsui, C.-Y. (2009) *Dual-power-path RF-DC multi-output power management unit for RFID tags*. *Proceedings of the IEEE Symposium on VLSI Circuits*, June, pp. 200–201.
[47] Rao, Y. and Arnold, D.P. (2011) An input-powered vibrational energy harvesting interface circuit with zero standby power. *IEEE Transactions on Power Electronics*, **26**(12), 3524–3533.
[48] Mandal, S. and Sarpeshkar, R. (2007) Low-power CMOS rectifier design for RFID applications. *IEEE Transactions on Circuits and Systems I: Regular Papers*, **54**(6), 1177–1188.
[49] Guo, S. and Lee, H. (2009) An efficiency-enhanced CMOS rectifier with unbalanced-biased comparators for transcutaneous-powered high-current implants. *IEEE Journal of Solid-State Circuits*, **44**(6), 1796–1804.
[50] Lu, Y., Ki, W.-H., and Yi, J. (2011) A 13.56 MHz CMOS rectifier with switched-offset for reversion current control. *Proceedings of the IEEE Symposium on VLSI Circuits*, June, pp. 246–247.
[51] Dwari, S. and Parsa, L. (2010) An efficient AC–DC step-up converter for low-voltage energy harvesting. *IEEE Transactions on Power Electronics*, **25**(8), 2188–2199.
[52] Kwon, D. and Rincon-Mora, G.A. (2010) A single-inductor AC–DC piezoelectric energy-harvester/battery-charger IC converting ±(0.35 to 1.2V) to (2.7 to 4.5V). *IEEE International Solid-State Circuits Conference (ISSCC)*, *Digest of Technical Papers*, San Francisco, CA, February 7–11, pp. 494–495.
[53] Huang, T.-C., Du, M.-J., Lin, K.-L., *et al*. (2014) A direct AC-DC and DC-DC cross-source energy harvesting circuit with analog iterating-based MPPT technique with 72.5% conversion efficiency and 94.6% tracking efficiency. *Proceedings of the IEEE Symposium on VLSI Circuits*, June, pp. 26–27.
[54] Erickson, R.W. and Maksimovic, D. (2001) *Fundamentals of Power Electronics*, 2nd edn. Kluwer Academic Publishers, Secaucus, NJ.
[55] Pylarinos, L. (2003) Charge Pumps: An Overview. http://www.eecg.utoronto.ca/~kphang/ece1371/chargepumps.pdf (accessed November 14, 2015).

[56] Favrat, P., Deval, P., and Declercq, M.J. (1998) High-efficiency CMOS voltage doubler. *IEEE Journal of Solid-State Circuits*, **33**(3), 410–416.

[57] Huang, T.-C., Du, M.-J., Yang, Y.-Y., *et al*. (2012) Non-invasion power monitoring with 120% harvesting energy improvement by maximum power extracting control for high sustainability power meter system. Proceedings of the IEEE Custom Integrated Circuits Conference (CICC), September, pp. 1–4.

[58] Paing, T., Shin, J., Zane, R., and Popovic, Z. (2008) Resistor emulation approach to low-power RF energy harvesting. *IEEE Transactions on Power Electronics*, **23**(3), 1494–1501.

[59] Enne, R., Nikolic, M., and Zimmermann, H. (2010) A maximum power-point tracker without digital signal processing in 0.35 μm CMOS for automotive applications. IEEE International Solid-State Circuits Conference (ISSCC), Digest of Technical Papers, February 7–11, pp. 494–495.